 doi:10.20944/preprints202203.0328.v1

Discovery of bispecific lead compounds from *Azadirachta indica* against ZIKA NS2B-NS3 Protease and RNA dependent RNA polymerase using molecular simulations

Sanjay Kumar [1,2], Sherif A. El-Kafrawy [3,4], Shiv Bharadwaj [5*], S. S. Maitra[1], Thamir A. Alandijany [3,4], Arwa A. Faizo [3,4], Aiah M. Khateb [3,6], Vivek Dhar Dwivedi [2*], Esam I. Azhar [3,4*]

[1]School of Biotechnology, Jawaharlal Nehru University, New Delhi 110067, INDIA.

[2]Center for Bioinformatics, Computational and Systems Biology, Pathfinder Research and Training Foundation, Greater Noida 201308, India.

[3]Special Infectious Agents Unit, King Fahd Medical Research Center, King Abdulaziz University, PO Box 128442, Jeddah 21362, Saudi Arabia,

[4]Department of Medical Laboratory Technology, Faculty of Applied Medical Science, King Abdulaziz University, Jeddah 21589, Saudi Arabia.

[5]Laboratory of Ligand Engineering, Institute of Biotechnology of the Czech Academy of Sciences, BIOCEV Research Center, Vestec, Czech Republic.

[6] Medical Laboratory Technology Department, College of Applied Medical Sciences, Taibah University, Madinah, Saudi Arabia, Medina 42353, KSA.

Corresponding Authors:

Esam I Azhar; Email: eazhar@kau.edu.sa

Shiv Bharadwaj; Email: shiv.bharadwaj@ibt.cas.cz

Vivek Dhar Dwivedi; Email vivek_bioinformatics@yahoo.com

Preprints (www.preprints.org) | NOT PEER-REVIEWED | Posted: 24 March 2022 doi:10.20944/preprints202203.0328.v1

Abstract

Zika virus (ZIKV) has been characterized as one of the potential pathogens and placed under future epidemic outbreaks by the WHO. However, lack of potential therapeutics can result in uncontrolled pandemic like other human pandemic viruses; therefore, prioritized effective therapeutics development has been recommended against ZIKV. In this context, the present study adopted the strategy to explore the lead compounds from *Azadirachta indica* against ZIKV via concurrent inhibition of the $ZIKV^{pro}$ and $ZIKV^{RdRp}$ proteins using molecular simulations. Initially, structure-based virtual screening of 44 bioflavonoids reported in *Azadirachta indica* against the crystal structures of targeted ZIKV proteins resulted in the identification of top four common bioflavonoids, viz. rutin, nicotiflorin, isoquercitrin, and hyperoside. These compounds showed substantial docking energy (-7.9 to -11.01 kcal/mol) and intermolecular interactions with essential residues of $ZIKV^{pro}$ (His^{51}, Asp^{74}, and Ser^{135}) and $ZIKV^{RdRp}$ (Asp^{540}, Ile^{799}, and Asp^{665}) by comparison to the reference compounds, O7N inhibitor ($ZIKV^{pro}$) and Sofosbuvir inhibitor ($ZIKV^{RdRp}$). Long interval molecular dynamics simulation (500 ns) on the selected docked poses reveals stability of respective docked complexes contributed by intermolecular hydrogen bonds and hydrophobic interactions. The predicted complex stability was further supported by calculated end-point binding free energy using molecular mechanics generalized born surface area (MM/GBSA) method. Consequently, the identified common bioflavonoids are recommended as promising therapeutic inhibitors of $ZIKV^{pro}$ and $ZIKV^{RdRp}$ for further experimental assessment.

KEYWORDS: Zika Virus, NS2B-NS3 Protease, RdRp, Therapeutics, Molecular dynamics, Flavonoids, *Azadirachta indica*

Preprints (www.preprints.org) | NOT PEER-REVIEWED | Posted: 24 March 2022 doi:10.20944/preprints202203.0328.v1

1. Introduction

Zika virus (ZIKV) was first isolated in 1947 from Zika forest, Uganda, East Africa [1], remained unnoticed for almost 60 years, and in 2007, when the first-ever epidemic outbreak occurred in Yap Island, Federated States of Micronesia, where 59 predictable and 49 confirmed Zika cases were reported [2], the virus caught everyone's attention. Since the first outbreak, the virus has crossed the boundaries and caused several epidemic outbreaks outside African countries in the last ten years, including the 2013-2014 outbreak in French Polynesia, infecting around 28,000 people [3,4]. The 2015 outbreak in Brazil resulted in suspected ZIKV disease in 440,000 to 1,300,000 people [5], and microcephaly and other neurological disorders were also associated in approximately 7,000 human populations [6,7]. In 2016, several cases of ZIKV infection in the US were observed in the females who never travelled to the countries affected with this virus, but their male partners did [8], and the presence of ZIKV in their semen confirmed that it could also be transmitted through sexual mode [9]. Similar to all the flaviviruses, ZIKV is also transmitted primarily through *Aedes aegypti* mosquitoes [10], but an additional and unique mode of sexual transmission [8] along with the vertical transmission from mother to fetus [11–13] makes this pathogen more notorious. The unavailability of vaccines and therapeutic drugs against the ZIKV makes this pathogen more threatening to humanity. It adds to the scientific community's challenges and opportunities in developing effective vaccine candidates and potential therapeutic drugs.

ZIKV is an enveloped flavivirus and encloses a 10.8 kb positive single-stranded RNA (+ssRNA) genome, which contains a single open reading frame (ORF) for the translation of a single polyprotein of 3419 amino acids [14]. Genome replication plays a central role in viral pathogenesis. Thus, after infection, ZIKV polyprotein is processed into three structural proteins (SPs): pre-membrane (prM), envelope (E), and capsid (C) proteins, and seven nonstructural proteins (NSPs): NS1, NS2A, NS2B, NS3, NS4A, NS4B, and NS5 via the proteolytic activity of both ZIKA and host proteinases (**Figure 1A**) [15]. The structural proteins protect the newly synthesized viral genome by forming an inner layer of capsid proteins and an outer lipid envelope derived from the host cell's heterodimeric prM-E protein complex. During maturation, the prM protein is cleaved into pr-subunit and M-subunit by the catalytic activity of host furin

Preprints (www.preprints.org) | NOT PEER-REVIEWED | Posted: 24 March 2022 doi:10.20944/preprints202203.0328.v1

protease in the trans-Golgi network (TGN). This results assist in releasing fully matured ZIKA virus with E and M protein on its outer envelope from the host cell [16]. Genome replication is the crux of viral pathogenesis and in the case of ZIKV, the NSPs interact to form a replication complex that provides a site for synthesizing viral genomic RNA. Among all the NSPs, NS3 ($ZIKV^{pro}$) and NS5 ($ZIKV^{RdRp}$) are the vital factors in ZIKV pathogenesis, as the former one is involved in genome replication due to its helicase activity and in post-translational processing of polyprotein due to its protease activity whereas the latter one has polymerase activity, which is required for the replication process [17].

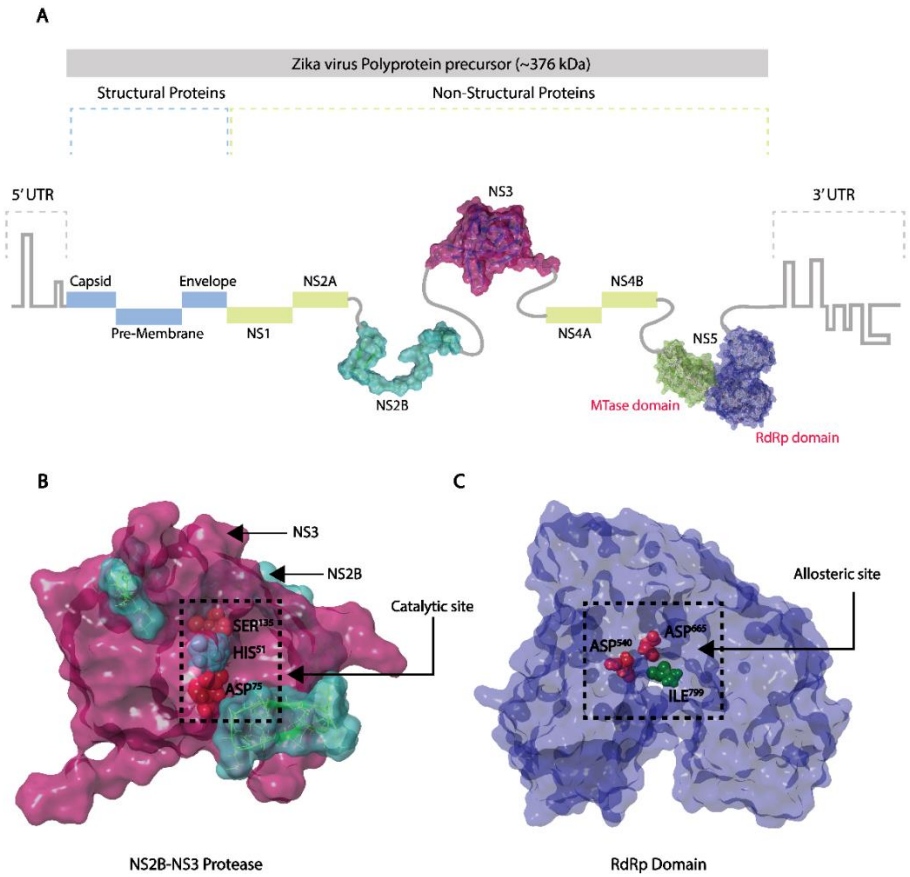

Figure 1. Zika virus protein structures**. A.** Arrangement of structural and non-structural proteins in a single polyprotein encoded by the ~10.8 kb RNA genome of Zika virus. **B.** Three-dimensional crystal structures of $ZIKV^{pro}$ of resolution 1.59 Å retrieved from the PDB with PDB ID: 6Y3B. **C.** Three-dimensional crystal structures of $ZIKV^{RdRp}$ of resolution 1.40 Å retrieved from Protein Data Bank (PDB) with PDB ID: 6LD2. (The 3D structures of proteins were prepared and modified using free Maestro academic version v12.9 package (**Schrödinger Release 2021-3**: Maestro, Schrödinger, LLC, New York, NY, 2021)

Preprints (www.preprints.org) | NOT PEER-REVIEWED | Posted: 24 March 2022 doi:10.20944/preprints202203.0328.v1

The ZIKV serine protease ($ZIKV^{pro}$) is a heterodimeric complex that consists of a membrane protein NS2B bound with ~70 kDa NS3 protein at the N-terminal residues possessing protease activity [18–20]. NS3 protein has a protease and helicase domain at N-terminal and C-terminal domains, respectively. However, despite lacking any enzymatic activity, NS2B plays a crucial role in the folding of NS3 protein [21–23], acted as a cofactor for the protease activity of NS3 [24], and holds NS3 protein near the cell membrane, which is essential for its proteolytic activity and viral replication [25–29]. Thus, in NS2B-NS3 protease ($ZIKV^{pro}$), the substrate binding and catalyzing active site of NS3 protease domain is enfolded by the NS2B protein, where a stretch of forty amino acid residues located at the C-terminal region of NS2B interact with the N-terminal protease domain of NS3 protein [30–35], resultant into the formation of a catalytic triad (His^{51}, Asp^{74}, and Ser^{135} residues), required for the proteolytic activity by the virus to release the functional NSPs in the cytosolic side of the host endoplasmic reticulum (ER) which further participate in viral replication (**Figure 1B**) [36] [37]. Due to its crucial role in the life cycle ZIKV and the lack of any alternative protease in human cells, $ZIKV^{pro}$ is considered a promising target for therapeutics. Additionally, NS5 is the largest and highly conserved protein among flaviviruses, which is a critical factor in the viral genome replication via the C-terminal RdRp domain; therefore, targeting the $ZIKV^{RdRp}$ has been considered as a precise therapeutic strategy against ZIKV [38–40]. The $ZIKV^{RdRp}$ protein possesses three subdomains where the "finger" and "thumb" subdomains intersect and create a tunnel resulting in the formation of an active site with a central catalytic pocket formed by the PALM subdomain. The amino acid residues ranging from 321 to 488 and 542 to 608 comprise finger domain, 484 to 541 and 609 to 714 comprise palm domain, and 715 to 903 comprise thumb domain, where Asp^{540} residue in PALM domain and, Ile^{799} and Asp^{665} residues in thumb domain are found in the catalytic site of $ZIKV^{RdRp}$ and crucial for interaction with the ligands (**Figure 1C**) [41,42]. In addition, NS5 protein also carries methyltransferase activity at the N-terminal end, which is required for the 5' capping of newly synthesized viral mRNA [43]. Hence, in the last five years after the WHO announced the ZIKV outbreak with a global health emergency in 2016, various orthosteric inhibitors [44,45], allosteric inhibitors [46–48], $ZIKV^{pro}$ inhibitors [49–51], $ZIKV^{RdRp}$ inhibitors [52–55], and a few inhibitors with

Preprints (www.preprints.org) | NOT PEER-REVIEWED | Posted: 24 March 2022 doi:10.20944/preprints202203.0328.v1

unknown molecular targets [56–58] were screened and tested against ZIKV infection. However, only one compound, viz. novobiocin, was noted for considerable *in vivo* inhibitory effect against the ZIKV infection [59]. In the war against ZIKV, a comprehensive blueprint needs to be comprised to develop promising therapeutics; thus, a multitargeted approach can be considered an aspiring strategy where the most appealing targets are $ZIKV^{pro}$ and $ZIKV^{RdRp}$ domains.

In the last two decades, multitargeted drugs have been preferred more due to their major advantages such as the lesser risk of drug interaction and improved drug compliance in patients [60–62]. Along with employing the multitargeting approach in this study, the compounds which have been selected for screening against the $ZIKV^{pro}$ and $ZIKV^{RdRp}$ domain of Zika virus (ZIKV) belong to the *Azadirachta indica,* which possess antibacterial, antifungal, and antiviral activity [63]. *A. indica* is famous as Neem, and its various parts such as leaves, flowers, bark, seeds, and roots have been used for therapy and treatment purposes against various infectious and non-infectious diseases in Asian and African countries since time immemorial. In recent few years, plants, especially *A. indica, are the foremost choice in finding a cure against various diseases because they are* much safer, readily available, affordable, and a long-term resource with constant mass production [64,65]. Therefore, in this study, 44 bioflavonoids reported from *Azadirachta indica,* were computationally screened against both the $ZIKV^{pro}$ and $ZIKV^{RdRp}$ to identify common potent inhibitors with substantial binding affinity and stability in the active pocket of selected ZIKV proteins.

2. Methodologies

2.1 Receptors and bioflavonoids

The three-dimensional (3D) crystal structure of Zika virus NS2B-NS3 protease ($ZIKV^{pro}$, PDB ID: 6Y3B [66]) and Zika virus RNA-dependent RNA polymerase domain ($ZIKV^{RdRp}$, PDB ID: 6LD2 [67]) collected at 1.59 and 1.40 Å resolutions, respectively were downloaded from the protein data bank (PDB) database (https://www.rcsb.org/) [68]. The selected proteins as receptors were preprocessed by assigning bond order and addition of hydrogen atoms using the protein preparation wizard of the Schrödinger maestro platform [69]. Following, protein structures were further treated for protonation of residues using the PROPKA program at pH 7.0, followed by

Preprints (www.preprints.org) | NOT PEER-REVIEWED | Posted: 24 March 2022 doi:10.20944/preprints202203.0328.v1

the restrained minimization using Optimized Potentials for Liquid Simulations 3e (OPLS3e) force field with default parameters.

To identify the secondary metabolites from *Azadirachta indica* (Neem plant) *as* putative inhibitors of ZIKV^{pro} and ZIKV^{RdRp}, a small library of known 44 bioflavonoids (**Table S1**) was prepared by exploring the documented research articles. The three-dimensional conformers of all bioflavonoids were retrieved from the PubChem database (https://pubchem.ncbi.nlm.nih.gov/) [70]. The ligand preparation was performed through LigPrep panel of Schrödinger (Schrödinger Release 2018-3: LigPrep, Schrödinger, LLC, New York, NY, 2018) using maestro platform by generating their tautomeric confirmers using EPIK state penalty at pH 7.0 ± 2.0 under OPLS3e force field. The grid was prepared using the Receptor Grid Generation panel of Schrödinger by selecting the 12 Å region around the active site residues of both the proteins and all other parameters followed the default settings in the Receptor Grid Generation.

2.2. Structure-based virtual screening and ADMET analysis

In the initial stages of drug discovery, structure-based virtual screening (SBVS) plays a crucial role in identifying bioactive therapeutic molecules against the three-dimensional structure of biological target proteins obtained through X-ray diffraction, NMR, Cryo-electron microscopy, or homology modelling. SBVS is a computational technique through which every compound/ligand from the selected database or library is docked with the active site of target proteins, and the compounds with high negative docking scores (binding energy) are selected for further in-silico, in-vivo, and in-vitro validation because the complex with higher negative binding energy possesses high binding affinity.

In search of common compounds from the library of 44 bioactive bioflavonoids from *Azadirachta indica,* SBVS was performed on the active pocket of the ZIKV^{pro} and ZIKV^{RdRp} using Glide extra precision (XP) module of Schrödinger suite (Schrödinger Release 2018-3**:** Glide, Schrödinger, LLC, New York, NY, 2018). The energy minimized structure of both the target proteins preprocessed through the Protein Preparation Wizard panel followed by the grid generation for ZIKV^{pro} and ZIKV^{RdRp} through Receptor Grid Generation panel and were imported

Preprints (www.preprints.org) | NOT PEER-REVIEWED | Posted: 24 March 2022 doi:10.20944/preprints202203.0328.v1

into the VSW panel along with the energy minimized ligands prepared through the LigPrep panel of the maestro, Schrödinger (Schrödinger Release 2018-3**:** LigPrep, Schrödinger, LLC, New York, NY, 2018). The grid was prepared around the catalytic site residues of $ZIKV^{pro}$ (Val^{36}, His^{51}, Asp^{75} Ser^{81}, Asp^{83}, Phe^{84}, Ser^{85}, Ser^{135} Asn^{152}, Gly^{153}, and Tyr^{161}) [66] and allosteric pocket of $ZIKV^{RdRp}$ (Asn^{612}, Asp^{665}, Asp^{666}, Cys^{711}, Thr^{796}, Try^{797}, Ser^{798}, And Ile^{799}, His^{800}) [71,72]. Based on docking score and EPIK state penalty, the top common bioflavonoids with significant binding scores were extracted as putative inhibitors of the selected proteins of ZIKV. Furthermore, collected bioflavonoids and respective reference compounds were computed for their pharmacokinetic/drug-like properties via ADMET analysis using SwissADME (http://www.swissadme.ch/) [73] and admetSAR (http://lmmd.ecust.edu.cn/admetsar2/) [74] online servers.

2.3. Redocking and intermolecular interaction profiling

The top common compounds collected from SBVS against ZIKV proteins, i.e., $ZIKV^{pro}$ and $ZIKV^{RdRp}$, and respective reference compounds, i.e., "O7N" (native ligand) for $ZIKV^{pro}$ and "Sofosbuvir" for $ZIKV^{RdRp}$ (previously reported nucleoside inhibitor of RdRp) [75], were redocked in the selected respective binding pockets of viral proteins under default parameters using Glide XP module of Schrödinger (Schrödinger Release 2018-3: Glide, Schrödinger, LLC, New York, NY, 2018). All the docked poses were studied for the intermolecular interactions under the default parameters of the Maestro v12.9 package and interaction images (3D and 2D) images were prepared using the free academic version of the Maestro v12.9 package.

2.4. Molecular dynamics simulation analysis

Dynamic stability and the intermolecular interactions profiling of the selected protein-ligand complexes were analyzed through the molecular dynamics simulation (MD simulation) using Free academic Desmond-maestro 2020-4 [76,77]. Initially, each docked complex was placed in a 10 Å x 10 Å x 10 Å orthorhombic box amended with explicit (TIP4P) solvent using a system builder module. Additionally, the complete simulation system was amended with 0.15 M salt to mimic the physiological conditions and neutralized using counter sodium and chlorine ions

Preprints (www.preprints.org) | NOT PEER-REVIEWED | Posted: 24 March 2022 doi:10.20944/preprints202203.0328.v1

while placed at 20 Å distance from the docked ligand in the receptor. Later, the simulation system was minimized under default parameters using a minimization tool and subjected to 500 ns MD simulation at 300K temperature and 1.01325 bar pressure with other default parameters using Free academic Desmond-maestro 2020-4 [76,77]. At last, the MD simulation trajectory of each protein-ligand complex was analyzed for the stability and intermolecular interactions as a function of 500 ns interval by simulation interaction diagram (SID) module in the Free academic Desmond-maestro 2020-4.

2.5. Endpoint Free binding energy calculation

Molecular mechanics/generalized Born Surface area (MMGBSA) was performed to calculate the mean binding free energy on the extracted poses from the last ten ns interval (at ten ps step) of respective MD simulation trajectory under default parameters of Prime MMGBSA module in Schrödinger suite (Schrödinger Release 2018-3: Prime, Schrödinger, LLC, New York, NY, 2018). Briefly, all the solvent molecules and ions were deleted for refining the extracted poses, as reported earlier (reference). Eventually, the net free binding energy (ΔG) was calculated using the following equation.

$$\Delta G_{Bind} = \Delta G_{Complex\ (minimized)} - \left(\Delta G_{\text{Complex (minimized)}} + \Delta G_{\text{Ligand (minimized)}}\right) \ldots (1)$$

Where ΔG_{Bind} = Binding free energy, $\Delta G_{\text{Complex (minimized)}}$ = Free energy of the complex, $\Delta G_{\text{Receptor (minimized)}}$ = Free energy for receptor, and $\Delta G_{\text{Ligand (minimized)}}$ = Free energy for ligand.

3. Results and discussion

3.1. Structure-based virtual screening

A small library of know bioflavonoids, 44 compounds belonging to the plant *Azadirachta indica* was used in the SBVS against the selected binding pocket of $ZIKV^{pro}$ and $ZIKV^{RdRp}$. The docking scores for all the screened compounds ranged between -2.0 to -11.01 kcal/mol, exhibiting interactions with essential residues of selected viral proteins (**Tables S2-S3**). Thus, based on their docking scores, only the top four common bioflavonoids were extracted for redocking and intermolecular interaction analysis (IMI analysis) against the reference inhibitor ligands of $ZIKV^{pro}$ and $ZIKV^{RdRp,}$ i.e., O7N and Sofosbuvir, respectively (**Figure 2**, **S2**). The primary goal of this study

Preprints (www.preprints.org) | NOT PEER-REVIEWED | Posted: 24 March 2022 doi:10.20944/preprints202203.0328.v1

was to find the common compounds from a natural source that can inhibit both the ZIKV^{pro} and ZIKV^{RdRp}. As anticipated, four bioactive bioflavonoids, i.e., Rutin, Nicotiflorin, Quercetin 3-beta-D-glucoside, and Hyperoside from the plant *Azadirachta indica,* were identified through Glide XP and each screened bioflavonoids showed a significant docking score (-7.9 to -11.01 kcal/mol) with the target proteins, i.e., ZIKV^{pro} and ZIKV^{RdRp} domain as mentioned in (**Table 1**). Interestingly, all the identified bioflavonoids were previously reported to have medicinal and therapeutic properties such as Rutin and Quercetin 3-beta-D-glucoside possessing antiviral, anticancer, and antidiabetic activities [78–85], Nicotiflorin was reported to inhibit SARS-CoV-2 M^{pro} [86,87], and Hyperoside was also reported to have anticancer activity [88,89].

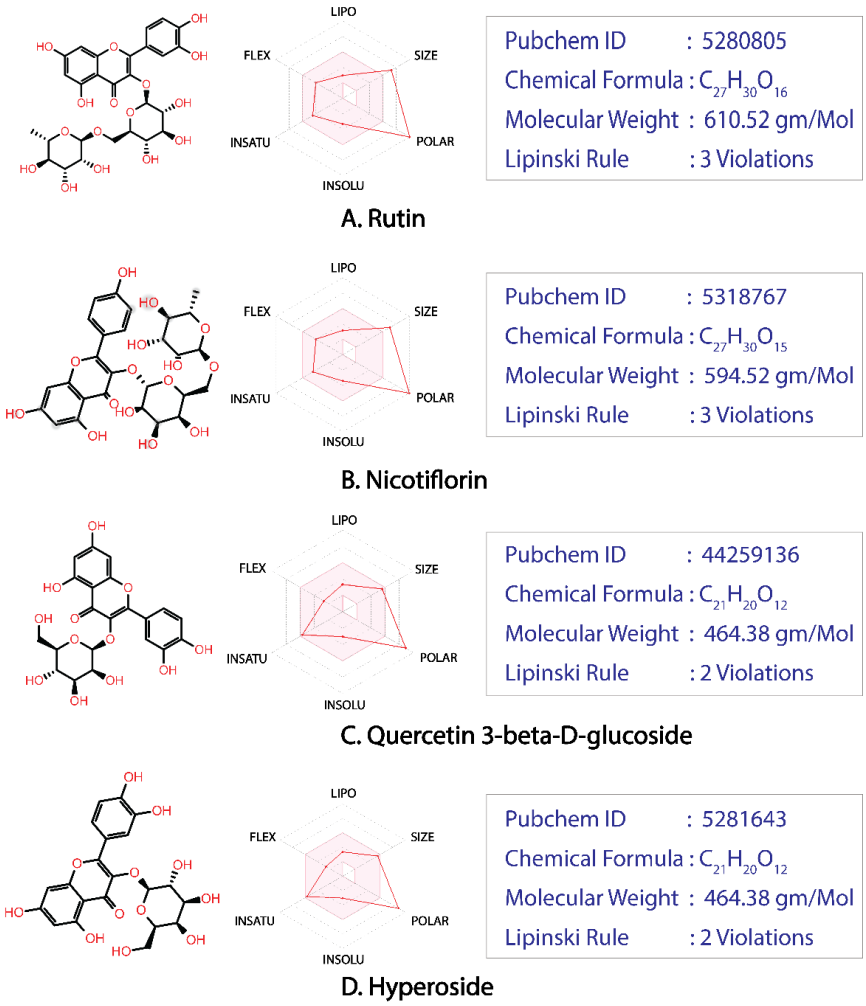

Figure: 2. 2D structures of selected common compounds and their ADMET analysis, i.e., **A.** Rutin **B.** Nicotiflorin **C.** Quercetin 3-beta-D-glucoside, and **D.** Hyperoside.

Preprints (www.preprints.org) | NOT PEER-REVIEWED | Posted: 24 March 2022 doi:10.20944/preprints202203.0328.v1

3.2. Redocking and intermolecular interaction analysis

Redocking is a mandatory post-SBVS step, which is required to assure that the compounds identified and selected through virtual screening have high affinity with the active site residues of the binding pocket because the algorithms of SBVS are fast and, therefore, its accuracy level is comparatively lower[90]. Thus, a stringent XP docking protocol was adopted in the redocking of the selected poses, and the most satisfactory binding poses with substantial binding affinity scores and interactions with the essential residues in the viral proteins, i.e., $ZIKV^{pro}$ and $ZIKV^{RdRp}$, were extracted for further analysis. Herein, the redocked complexes of $ZIKV^{pro}$ with rutin, nicotiflorin, Quercetin 3-beta-D-glucoside, and Hyperoside were noted for -10.61, -9.95, -8.63, and -8.37 kcal/mol, respectively, whereas in complexed with $ZIKV^{RdRp}$, the docking score showed by rutin, nicotiflorin, Quercetin 3-beta-D-glucoside, and Hyperoside were -11.01, -10.56, -8.84, and -7.87 kcal/mol respectively (**Table 1**). Interestingly, all four bioactive bioflavonoids, i.e., Rutin, Nicotiflorin, Quercetin 3-beta-D-glucoside, and Hyperoside, showed significant docking scores (-7.8 to 11.01 kcal/mol) with both the target proteins in comparison to the docking scores of reference inhibitors, O7N for $ZIKV^{pro}$-O7N inhibitor (-6.629 Kcal/mol) and $ZIKV^{RdRp}$-Sofosbuvir inhibitor (-6.033 Kcal/mol). The redocking results concluded that each of the selected bioflavonoids showed a considerable binding affinity with the binding pocket of selected viral targets, i.e., $ZIKV^{pro}$ and $ZIKV^{RdRp}$.

IMI analysis was required to understand the interactions profile between the selected ligands (rutin, nicotiflorin, quercetin 3-beta-D-glucoside, and hyperoside) and the target proteins ($ZIKV^{pro}$ and $ZIKV^{RdRp}$). Mainly hydrogen bonds, salt bridge, and pi-pi interactions were observed in all the interactions between target proteins ($ZIKV^{pro}$ and $ZIKV^{RdRp}$) and selected ligands (rutin, nicotiflorin, Quercetin 3-beta-D-glucoside, and Hyperoside). The docked complex, $ZIKV^{pro}$-Rutin, is stabilized via four hydrogen bonds (with residues Val^{36}, Ser^{81}, Asn^{152}, and Gly^{153}), and two pi-pi stacking interactions (with His^{51}) (**Figure 3A and 3B**). $ZIKV^{pro}$-Nicotiflorin is stabilized via five hydrogen bonds (with residues Val^{36}, Ser^{81}, Asn^{152}, Gly^{153}, and Tyr^{161}) and two pi-pi stacking interactions (with His^{51} residue) (**Figure 3C and 3D**). $ZIKV^{pro}$-Quercetin 3-beta-D-glucoside is stabilized via six hydrogen bonds with four residues (Asp^{83}, Phe^{84}, Gly^{153}, and Asn^{152}) and one hydrophobic bond with Tyr^{161} (**Figure 3E and 3F**). $ZIKV^{pro}$-Hyperoside is stabilized via five

Preprints (www.preprints.org) | NOT PEER-REVIEWED | Posted: 24 March 2022 doi:10.20944/preprints202203.0328.v1

hydrogen bonds (Val[36], Asp[75], Asp[83], Tyr[150], and Gly[153]), two pi-pi stacking interactions with His[51] residue, and one hydrophobic interaction Tyr[161] (**Figure 3G and 3H**).

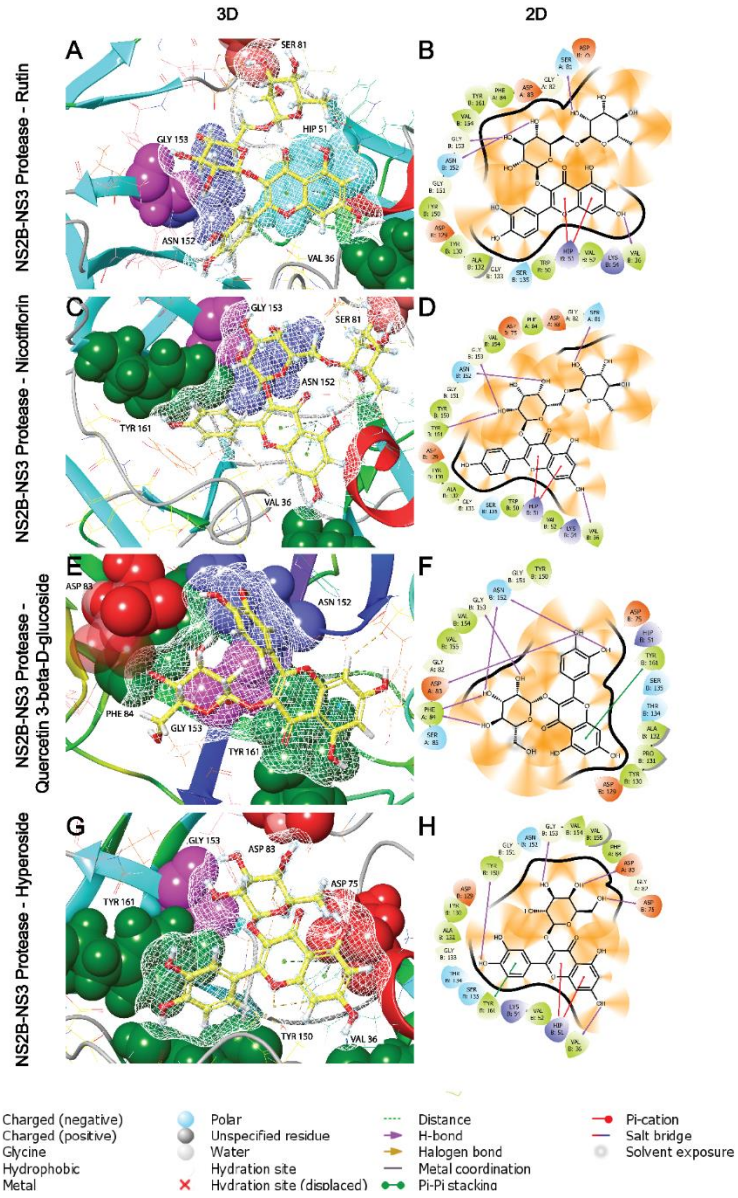

Figure 3. 3D and 2D interaction profiles for ZIKV[pro] -ligands; **A-B.** ZIKV[pro] -Rutin, **C-D.** ZIKV[pro] -Nicotiflorin, **E-F.** ZIKV[pro] -Quercetin 3-beta-D-glucoside, and **G-H.** ZIKV[pro] -Nicotiflorin, depicting active residues around the ligand at 4 Å area in the active pocket of ZIKV[pro].

Docked complex ZIKV[RdRp]-Rutin is stabilized with seven hydrogen bonds with five amino acid residues with Glu[419], Gly[604], Asp[666], Ser[798], and Ile[799], two hydrophobic bonds with Trp[797] (**Figure 4A and 4B**). Docked complex ZIKV[RdRp]-Nicotiflorin is stabilized by forming six hydrogen bonds

Preprints (www.preprints.org) | NOT PEER-REVIEWED | Posted: 24 March 2022 doi:10.20944/preprints202203.0328.v1

with residues Asp^{540}, Trp^{539}, Asp^{665}, Asp^{666}, and Cys^{711} (**Figure 4C and 4D**). Likewise, docked complex ZIKV^{RdRp}-Quercetin 3-beta-D-glucoside also included only hydrogen bonds for its stabilization with residues Asp^{540}, Asp^{665}, Asp^{666}, Cys^{711}, and ILE^{799} (**Figure 4E and 4F**). Compared to other complexes, ZIKV^{RdRp}-Hyperoside docked complex included only two amino acid residues (Asp^{540}, and Asp^{666}) for hydrogen bonding (**Figure 4G and 4H**). The same amino acid composition was also observed in the intermolecular interactions of reference docked complex, i.e., ZIKV^{pro}-O7N and ZIKV^{RdRp}-Sofosbuvir (**Supplementary Figure S1**).

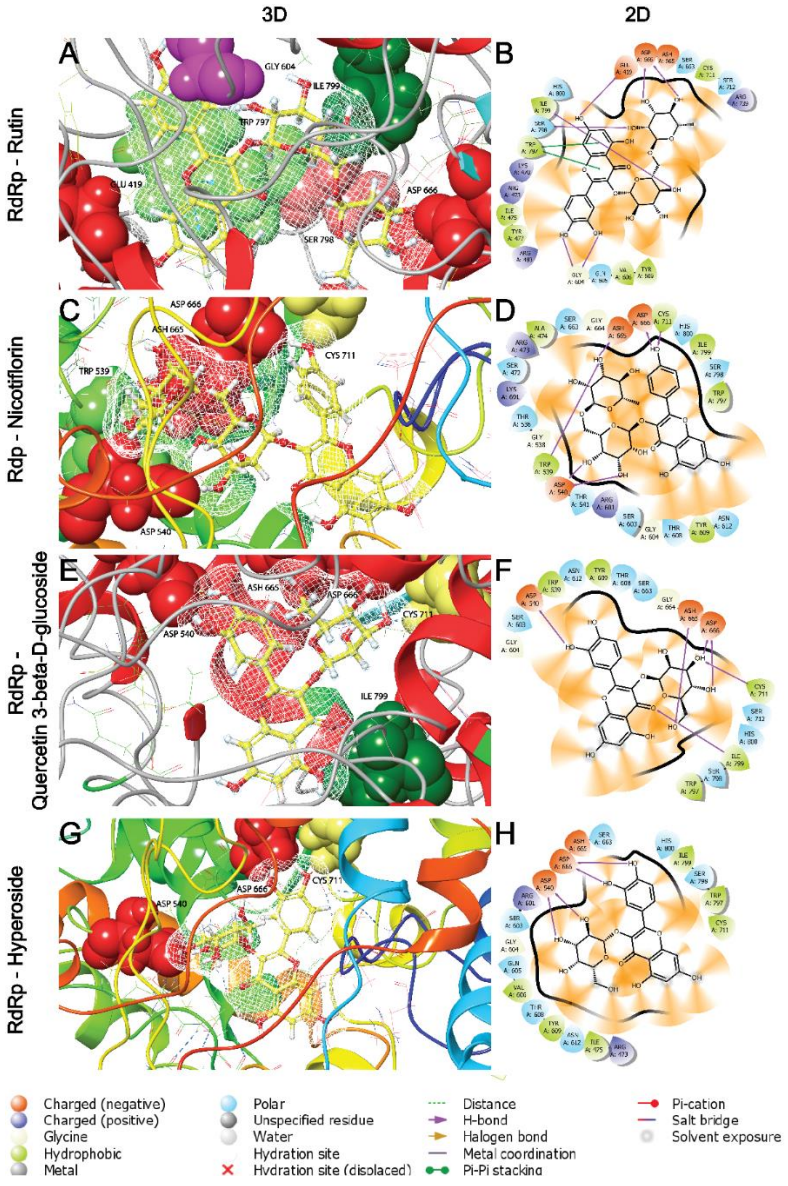

Figure 4. 3D and 2D interaction profiles for ZIKV^{RdRp}-ligands; **A-B.** ZIKV^{RdRp}-Rutin, **C-D.** ZIKV^{RdRp}–Nicotiflorin, **E-F.** ZIKV^{RdRp}-Quercetin 3-beta-D-glucoside, and **G-H.** ZIKV^{RdRp}-Nicotiflorin, depicting active residues around the ligand at 4 Å area in the active pocket of ZIKV^{RdRp}.

Preprints (www.preprints.org) | NOT PEER-REVIEWED | Posted: 24 March 2022 doi:10.20944/preprints202203.0328.v1

Table 1. Redocking score and intermolecular interactions noted for the screened compounds with the viral proteins, i.e., ZIKV^{pro}and ZIKV^{RdRp}, within 4 A around the docked ligand in the respective binding pockets.

S. no.	Compounds	Redocking Score (kcal/mol)		Hydrogen bond		π-π stacking/ Salt bridge		Hydrophobic	
		ZIKV^{pro}	ZIKV^{RdRp}	ZIKV^{pro}	ZIKV^{RdRp}	ZIKVpro	ZIKV^{RdRp}	ZIKV^{pro}	ZIKV^{RdRp}
1.	Rutin	-10.645	-11.038	Val^{36}, Ser^{81}, Asn^{152}, Gly^{153}	Glu^{419}, Gly^{604}, Asp^{666}, Ser^{798}, Ilu^{799}	His^{51}	-	-	Trp^{797}
2.	Nicotiflorin	-9.986	-10.593	Val^{36}, Ser^{81}, Asn^{152}, Gly^{153}, Tyr^{161}	Trp^{539}, Asp^{540}, Ash^{665}, Asp^{666}, Cys^{711}	His^{51}	-	-	-
3.	Quercetin 3-beta-D-glucoside	-8.666	-8.877	Asp^{83}, Phe^{84}, Asn^{152}, Gly^{153}	Asp^{540}, Ash^{665}, Asp^{666}, Cys^{711}, Ilu^{799}	-	-	Tyr^{161}	-
4.	Hyperoside	-8.4	-7.907	Val^{36}, Asp^{75}, Asp^{83}, Tyr^{150}, Gly^{153}	Asp^{540}, Asp^{666}	His^{51}	-	Tyr^{161}	-

3.3. ADMET and drug-likeliness analysis

In the field of drug discovery, the molecules proposed as a drug candidate must carry high biological activity and less toxicity. Therefore, a few critical pharmacological parameters, such as absorption, distribution, metabolism, excretion, and toxicity (ADMET parameters) along with the pharmacokinetics, must be validated for every proposed drug candidate. This is because the early assessments of such parameters in the initial phase of drug discovery essentially contribute to understanding and lowering the pharmacokinetic-related failure of drugs in the later phase during clinical trial [91]. To analyze the pharmacokinetic properties and drug-likeness, all the screened bioactive bioflavonoids, i.e., Rutin, Nicotiflorin, Quercetin 3-beta-D-glucoside, and Hyperoside, as well as the reference inhibitors, i.e., O7N (for ZIKV^{pro}) and Sofosbuvir (for ZIKV^{RdRp}) (**Figure 2 and Supplementary Figure S2**) were uploaded on the SwissADME and admetSAR online servers and allowed for the assessment of their ADMET properties. Interestingly, all the bioflavonoids showed negative AMES toxicity test and non-carcinogenic profile via admetSAR server.

Moreover, selected bioflavonoids were found to be non-inhibitor of several cytochromes such as CYP2D6, CYP1A2, CYP2C19, CYP2C9, CYP2D6, CYP3A4, which plays a crucial role in the metabolism of drugs as well as various xenobiotics, and inhibition of this cytochromes may lead to the reduced drug efficacy, drug activation, and drug metabolism. Notably, all four identified

Preprints (www.preprints.org) | NOT PEER-REVIEWED | Posted: 24 March 2022 doi:10.20944/preprints202203.0328.v1

bioflavonoids also exhibit low gastrointestinal absorption along with a lack of Blood-Brain Barrier (BBB) permeability. However, Rutin and Nicotiflorin show three violations, whereas Quercetin 3-beta-D-glucoside and Hyperoside show two violations against Lipinski's rule of five (**Supplementary Table S4 and S5**). The selected bioflavonoids also showed violations against several other rules related to drug-likeness, such as Ghose, Veber, Egan, and Muegge. However, the rules for drug-likeness are not mandatory to be fulfilled by natural compounds as cells recognize these natural compounds through the active transport system [92,93]. Additionally, several other properties related to medicinal chemistry and pharmacokinetics were evaluated for potential compounds (Supplementary Table S3 and S4). Conclusively, the identified bioflavonoids against the ZIKV^{pro} and ZIKV^{RdRp} were suggested to be possessing ideal medicinal properties.

3.4. Long interval molecular dynamics simulation

In the field of drug discovery through computational approaches, MD simulation is an imperative technique by which the dynamic stability and the formation of intermolecular interactions of docked protein-ligand complexes are analyzed with respect to time. In this study, two different Zika proteins, ZIKV^{pro} and ZIKV^{RdRp} were found to interact with four common bioflavonoids (rutin, nicotiflorin, quercetin 3-beta-D-glucoside, and hyperoside) with significant binding energy from plant *Azadirachta indica,* and the resultant complexes ZIKV^{pro}-Rutin and ZIKV^{RdRp}-Rutin, ZIKV^{pro}-Nicotiflorin and ZIKV^{RdRp}-Nicotiflorin, ZIKV^{pro}-Quercetin 3-beta-D-glucoside and ZIKV^{RdRp}-Quercetin 3-beta-D-glucoside, ZIKV^{pro}-Hyperoside, and ZIKV^{RdRp}-Hyperoside) were simulated in the presence of a solvent, temperature, and pressure for the period of 500 ns to analyze their stability and intermolecular interaction genesis (**Figure 5, 6, and 7**). Similarly, by applying the same parameters, the reference docked complexes, ZIKV^{pro}-O7N, and ZIKV^{RdRp}-Sofosbuvir were also allowed to go through the simulation for comparing the stability and interaction pattern of experimented docked complexes (**Figure S3 and S6**).

At first, stability and steadiness of ligands in the binding pocket of respective target proteins (ZIKV^{pro} and ZIKV^{RdRp}) were observed at the end of 500 ns simulation compared to the initial frame, which revealed that the conformation of proteins and ligands slightly changed during the

Preprints (www.preprints.org) | NOT PEER-REVIEWED | Posted: 24 March 2022 doi:10.20944/preprints202203.0328.v1

simulation. However, the binding and stability of all the flavonoid ligands (rutin, nicotiflorin, quercetin 3-beta-D-glucoside, and hyperoside) in the active site of both the target proteins, i.e., ZIKV^{pro} (**Figure 5**) and ZIKV^{RdRp} (**Figure 6**) were significantly stable and steady similar to the reference inhibitors. In addition, with the analysis of intermolecular interactions, other important properties such as root mean square deviation (RMSD), root mean square fluctuation (RMSF), and protein-ligand contact mapping, were extracted from the MD trajectory for each complex in support of the simulation interaction diagram in Maestro-Desmond interface.

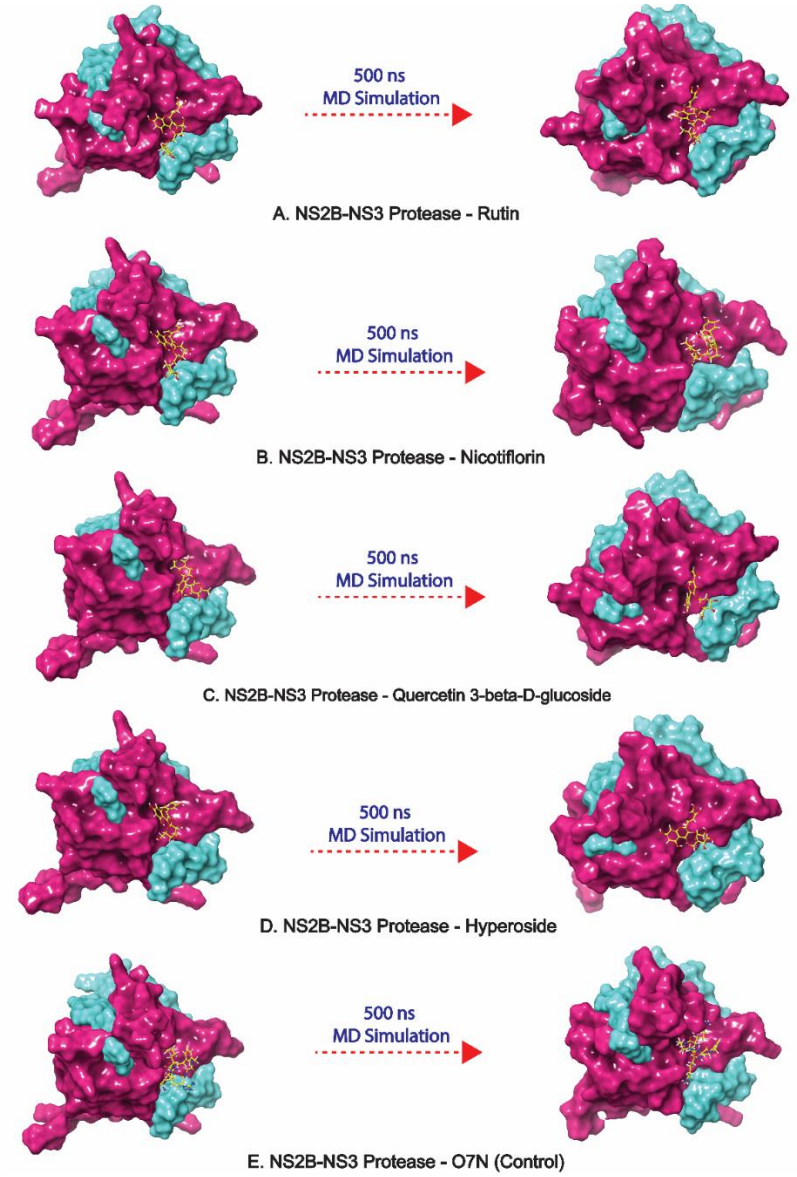

Figure 5. 3D docked poses of ZIKV^{pro}-natural compounds, i.e., **A.** ZIKV^{pro}-Rutin, **B.** ZIKV^{pro}-Nicotiflorin, **C.** ZIKV^{pro}-Quercetin 3-beta-D-glucoside, **D.** ZIKV^{pro}-Hyperoside, **E.** ZIKV^{pro}- O7N, exhibiting transition of docked posed through 500 ns MD simulation interval.

Preprints (www.preprints.org) | NOT PEER-REVIEWED | Posted: 24 March 2022 doi:10.20944/preprints202203.0328.v1

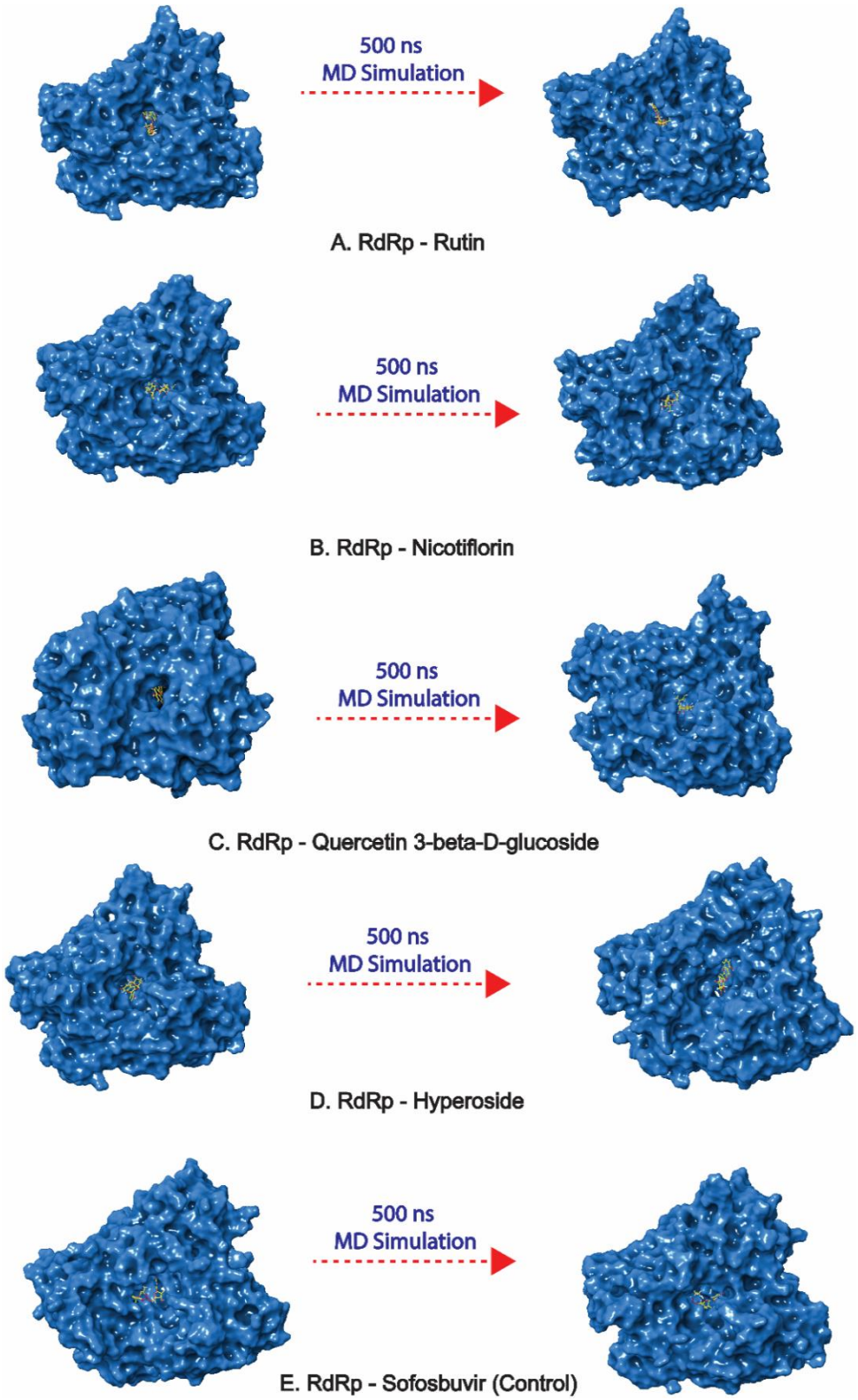

Figure 6. 3D docked poses of ZIKV^{RdRp}-natural compounds, i.e., **A.** ZIKV^{RdRp}-Rutin, **B.** ZIKV^{RdRp}-Nicotiflorin, **C.** ZIKV^{RdRp}-Quercetin 3-beta-D-glucoside, **D.** ZIKV^{RdRp}-Hyperoside, **E.** ZIKV^{RdRp}-Sofosbuvir, exhibiting transition of docked posed through 500 ns MD simulation interval.

Preprints (www.preprints.org) | NOT PEER-REVIEWED | Posted: 24 March 2022 doi:10.20944/preprints202203.0328.v1

3.4.1. RMSD and RMSF analysis

The following equation calculated the Root Mean Square Deviation (RMSD) values for the protein structure and the bound ligand from each frame during the 500 ns simulation trajectory to measure the average deviation that occurred in the protein and ligand structure for the respective docked complex in reference to the initial frame [86].

$$\mathrm{RMSD}_x = \sqrt{\frac{1}{N}\sum_{i=1}^{N}\left(r'_i\,(t_x) - r_i(t_{ref})\right)^2} \quad \ldots (2)$$

While calculating RMSD, *N* represents the number of atoms selected; t_{ref} is defined as reference time at zero interval; r′ denotes the position of the atoms under evaluation in frame x followed by the superimposition on the reference frame at time interval t_x. Moreover, Root Mean Square Fluctuation (RMSF) values were also calculated for characterizing the local fluctuations at residue and atomic level in protein chain and ligand molecule, respectively. The following equation expresses the local fluctuation in the simulation trajectory [86].

$$\mathrm{RMSF}_i = \sqrt{\frac{1}{T}\sum_{t=1}^{T}\left(r'_i\,(t) - r_i(t_{ref})\right)^2} \ldots (3)$$

While calculating RMSF, T denotes the simulation interval for which the RMSF is calculated, t_{ref} denotes the reference time, r_i denotes the atom (i) position in reference time t_{ref} and r′ denotes atom (i) position at the time following superimposition on the reference frame.

Initially, the protein and ligand RMSD for the docked complexes of potential bioflavonoids with the $ZIKV^{pro}$ and $ZIKV^{RdRp}$ were analyzed with respect to the initial pose as a reference frame (**Figure 7**). In all the $ZIKV^{pro}$-ligand docked complexes, $ZIKV^{pro}$ showed deviation in the considerable range of <2.8 Å till 500 ns simulation time interval (**Figure 7A-7D**) like $ZIKV^{pro}$ in the docked complex reference $ZIKV^{pro}$-O7N inhibitor complex (**Figure S3A**). In comparison to the reference O7N inhibitor docked with ZIKVpro, which showed deviations after 400 ns simulation time up to 5.6 Å and remained deviated till the end of 500 ns simulation (**Figure S2A**), all the selected ligands (Rutin, Nicotiflorin, Quercetin 3-beta-D-glucoside, and Hyperoside) showed deviation in the considerable range of <4.8 Å (**Figure 7A-7D**). These observations were further supported by the respective RMSF values of proteins (<2.8 Å) and ligands (<4.0 Å) (**Figure S4 and S5**).

Preprints (www.preprints.org) | NOT PEER-REVIEWED | Posted: 24 March 2022 doi:10.20944/preprints202203.0328.v1

Similarly, in case of all the ZIKV^{RdRp}-ligand docked complexes, the ZIKV^{RdRp} showed the deviation in the considerable range of <2.8 Å till 500 ns (**Figure 7E-7H**).However, in comparison to the reference inhibitor 'sofosbuvir' docked with ZIKV^{RdRp} showing deviation <5.0 Å along with the stable trajectory till 500 ns simulation time (**Figure S3B**), all the ligands showed deviation >5.0 Å up to 6 to 7 Å except Rutin which showed deviation in the considerable range of <5.0 Å (**Figure 7E-7H**) similar to the reference sofosbuvir inhibitor (**Figure S3B**). The high deviation of nicotiflorin, Quercetin 3-beta-D-glucoside, and Hyperoside in the docked complex with the ZIKV^{RdRp} was due to their internal atomic fluctuation, was supported by respective RMSF values (>4.0 Å). In contrast, the RMSF value of Rutin was relatively lower (<2.0 Å), which showed less deviation (**Figure S5F-S5J**). Overall, the stability and the rigidity of proteins and ligands in all the complexes were significantly acceptable, and no structural deformation was noticed in the target protein structure.

Preprints (www.preprints.org) | NOT PEER-REVIEWED | Posted: 24 March 2022 doi:10.20944/preprints202203.0328.v1

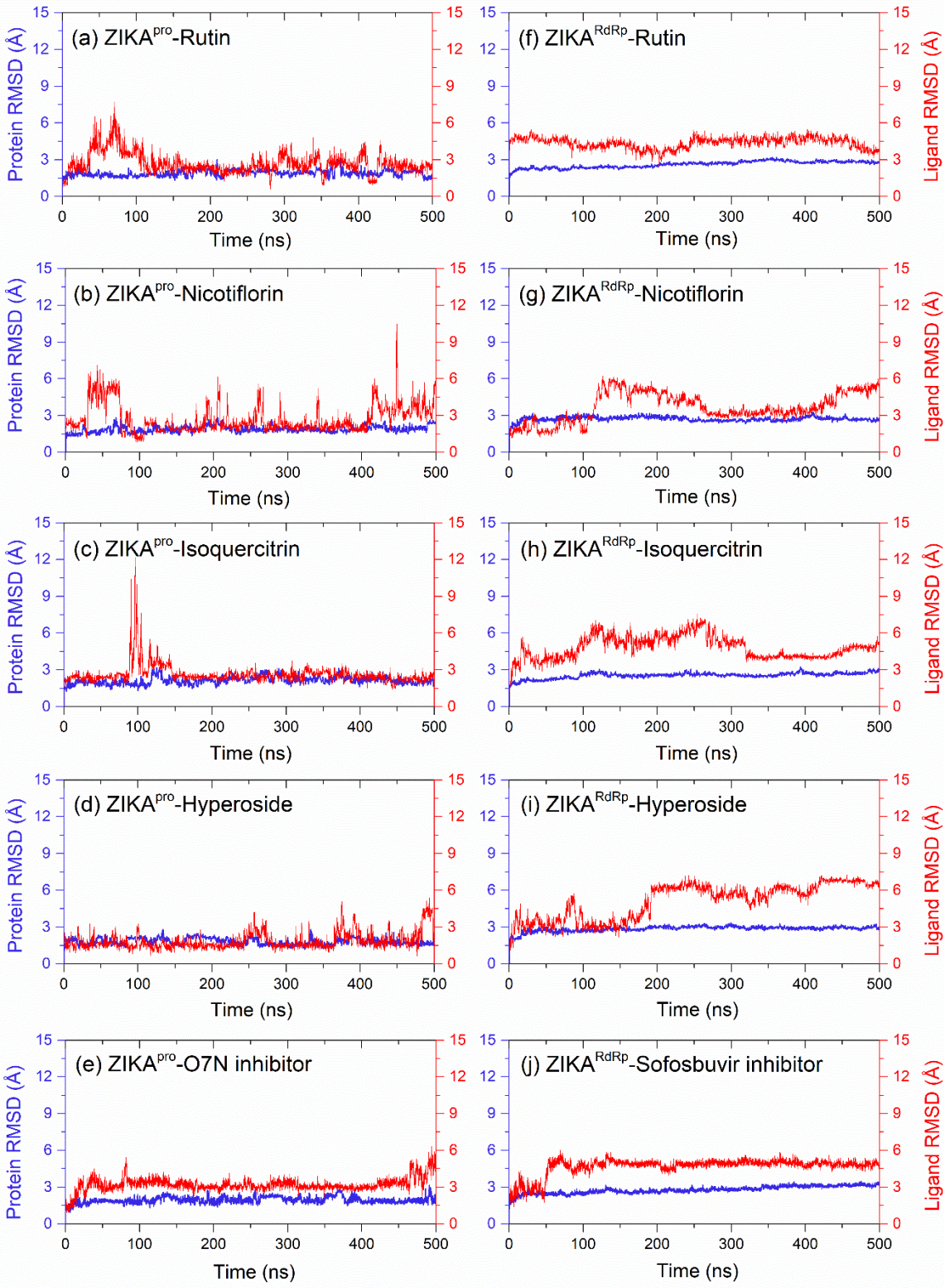

Figure 7. RMSD values were extracted for alpha carbon atoms (blue curves) of ZIKV^{pro} and ZIKV^{RdRp} domain, whereas natural compounds (red curves) from the 500 ns MD simulation of the respective complexes.

Preprints (www.preprints.org) | NOT PEER-REVIEWED | Posted: 24 March 2022 doi:10.20944/preprints202203.0328.v1

3.4.2. Protein-Ligand Interaction profiling

In the protein-ligand interaction, non-covalent bonding, especially hydrogen bonding and other interactions such as hydrophobic interaction, ionic interactions, pi-pi stacking, salt bridges, and water bridges formation, plays a vital role in providing stability to the complex. Therefore, in addition to the RMSD and RMSF analysis during 500 ns simulation interval, protein-ligand contact profiling was also observed by extracting the intermolecular interactions for all the docked ZIKV^{pro}-Ligand and ZIKV^{RdRp}-Ligand complexes against the reference docked complexes, i.e., ZIKV^{pro}-O7N inhibitor and ZIKV^{RdRp}-Sofosbuvir inhibitor, respectively, concerning the formation of different types of non-covalent interactions (**Figure 8, 9, and Supplementary Figures S6-S8**).

In the case of ZIKVpro-ligand docked complexes, all the selected bioflavonoids ligands (Rutin, Nicotiflorin, Quercetin 3-beta-D-glucoside, and Hyperoside) showed significant intermolecular contact formation against reference inhibitor O7N. In comparison to the initial ZIKV^{pro}-Ligand docked complexes where the residues of ZIKV^{pro} (Ser^{81}, Val^{36}, His^{51}, Asp^{75}, Asp^{83}, Phe^{84}, Asn^{152}, Gly^{153}, and Tyr^{161}) involved in the interaction with different flavonoid ligands (**Figure 3**), the identical residues were found to be involved in the intermolecular interactions during 500 ns simulation which confirms the dynamic stability of all the identified flavonoid ligands within the binding pocket of ZIKV^{pro}. His^{51} was observed to be involved in the formation of hydrophobic interaction for more than 50% in case of all ZIKV^{pro}-ligand complexes except with rutin. Similarly, TYR^{161} was also observed to form hydrophobic interactions for more than 40% of the simulation time in the case of rutin and nicotiflorin whereas, in the case of other two ligands (Quercetin 3-beta-D-glucoside and Hyperoside), it showed hydrophobic interaction for more than 90% of the simulation time. Gly^{153} was observed to form mainly H-bond in the case of rutin and nicotiflorin only, whereas Tyr^{130} appeared as a naïve interacting residue during the simulation in the case of all the ZIKV^{pro}-Ligand docked complexes. Along with the hydrogen and hydrophobic interactions, several residues such as Ser^{81}, Asp^{83}, Phe^{84}, Val^{72}, Asp^{75}, and Gly^{153} were observed to form ionic interactions for a shorter period, but these flashy ionic interactions might be crucial for the stability of ligands in the active binding pocket (**Figure 8**). Few interacting residues, such as Asp^{75}, Asp^{83}, Try^{130}, Gly^{153}, and Tyr^{161}, were observed as common in the intermolecular

Preprints (www.preprints.org) | NOT PEER-REVIEWED | Posted: 24 March 2022 doi:10.20944/preprints202203.0328.v1

interactions of the reference ZIKV^{pro}-O7N docked complex. In the reference docked ZIKV^{pro}-O7N complex, ASP^{83} (chain A) were observed to form two hydrogen bonds with the ligand for more than 100%, Ser8^{1} (chain A), Asp^{75} (chain B), Asp^{129} (chain B), Tyr^{130} (chain B), Gly^{153} (chain B), and Tyr^{161} (chain B) formed single hydrogen bond for more than 50% of the 500 ns simulation time. All these residues required a water bridge to form hydrogen bonds. Tyr^{161} (chain B), along with the H-bond for more than 90%, also formed a hydrophobic bond for more than 50% of the 500 ns simulation time, whereas Val^{155} (chain B) were involved in the formation of only hydrophobic interaction for more than 50% of the simulation time (**Figure S6**).

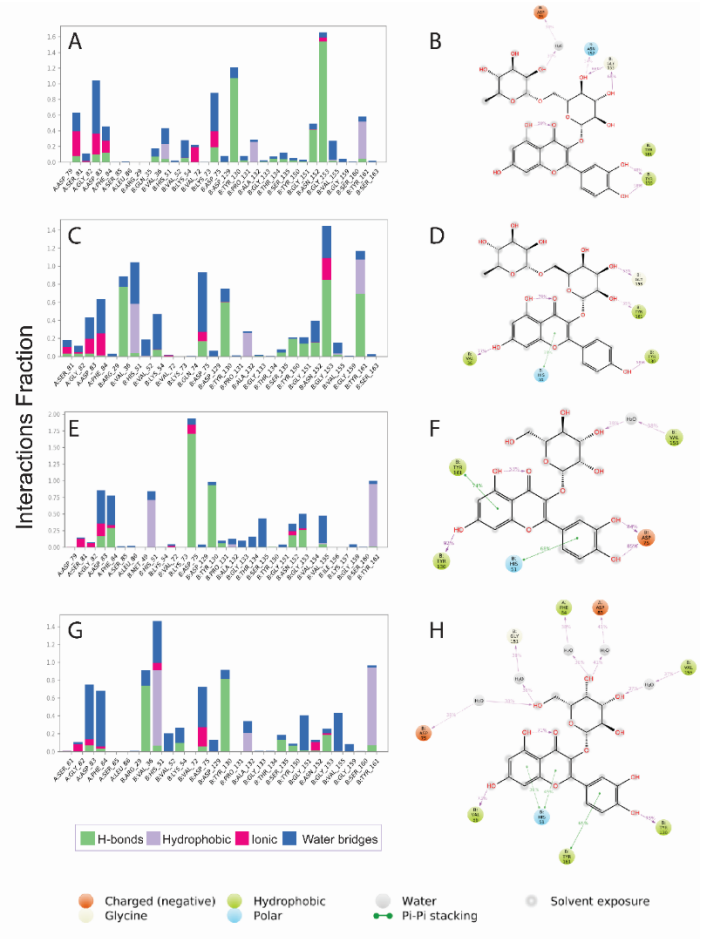

Figure 8. Protein-ligand interactions mapping for ZIKV^{pro} with selected natural compounds, i.e. **A-B.** Rutin, **C-D.** Nicotiflorin, **E-F.** Quercetin 3-beta-D-glucoside, and **G-H.** Hyperoside, extracted from 500 ns MD simulations. In the 2D interaction diagram, the residues tyrosine, Valine, and Phenylalanine (green), Aspartic acid (red), histidine and asparagine (blue), and glycine (grey) exhibit the hydrophobic, negative, polar, and non-polar interactions, respectively, along with hydrogen bonding (pink arrow) and pi-pi stacking (green line) with the receptor are extracted at 30% of the total MD simulation interaction interval.

Preprints (www.preprints.org) | NOT PEER-REVIEWED | Posted: 24 March 2022 doi:10.20944/preprints202203.0328.v1

During the analysis of protein-ligand contact profiling of ZIKV^{RdRp}-Ligand docked complex during simulation, it was observed that in ZIKV^{RdRp}-Rutin docked complex, Glu^{419}, Gly^{604}, Trp^{797}, and Ser^{798} residues were remain involved in the intermolecular interactions along with the addition of a few more interacting residues such as Ile^{475} (formed hydrophobic interaction for more than 75% of simulation time), Arg^{483} (formed hydrogen bond for more than 100% and hydrophobic interaction for ~30% of the simulation time) interaction during the 500 ns simulation (**Figure 9A-9B**). In ZIKV^{RdRp}-Nicotiflorin docked complex, Trp^{539}, Asp^{540}, and Asp^{665} remain involved in the interaction with the ligand along with the addition of a few more interacting residues such as Thr^{608} (formed hydrogen bond for 90% of simulation time), Tyr^{609} (formed hydrophobic interaction for more than 75% of the simulation time), and Trp^{797} (formed hydrophobic interaction for more than 100% of the simulation time) with the help of water bridge (**Figure 9C-9D**). In ZIKV^{RdRp}-Quercetin 3-beta-D-glucoside docked complex, Asp^{665}, Asp^{666}, and Ile^{799} were remained involved in the interactions along with the addition of a few more interacting residues during the 500 ns simulation, such as Ser^{472} (formed hydrogen bond for more than 20% of the simulation time), Glu^{509} (formed hydrophobic interaction for more than 30% of the simulation time), Tyr^{609} (formed hydrophobic interaction for more than 40% of the simulation time), Ser^{663} (formed hydrogen bond for more than 40% of the simulation time) with the help of water bridge (**Figure 9E-9F**). In ZIKV^{RdRp}-Hyperoside docked complex, the initially interacting residues Asp^{540}, Asp^{666}, and Cys^{711} were involved in the interaction during the simulation for a significantly shorter time. However, this complex developed some stronger interactions during the 500 ns simulation, such as Arg^{473} (formed bonds for more than 40% of the simulation), Trp^{476} (formed two hydrogen bonds for more than 55% of the simulation), Ser^{603} (formed hydrogen bond for more than 50% of the simulation), Arg^{794} (formed two hydrogen bonds for 40% of the simulation), and Trp^{797} (formed hydrophobic interaction for more than 75% of the simulation) with the help of water bridge (**Figure 9G-9H**). However, in the reference, ZIKV^{RdRp} -Sofosbuvir docked complex, Arg^{473}, Thr^{796}, and Ser^{798} were observed to form hydrogen bonds, and Arg^{739} formed hydrophobic interaction, and several residues were also involved in water bridge formation (**Figure S6B**). Hence, these results are encouraging evidence of stability between the identified flavonoid ligands (Rutin, Nicotiflorin, Quercetin 3-beta-D-glucoside, and

Preprints (www.preprints.org) | NOT PEER-REVIEWED | Posted: 24 March 2022 doi:10.20944/preprints202203.0328.v1

Hyperoside) and the target proteins (ZIKV^{pro} and ZIKV^{RdRp}) of the Zika virus. Additionally, the information related to the total number of residues involved in the intermolecular interaction were extracted 500 ns simulation along with their interaction density represented with the orange colour bands (dark colour represents the multiple contacts of the ligand with the protein residues on a particular frame) (**Supplementary Figures S7 and S8**). Furthermore, intermolecular interactions of the selected potential bioflavonoids, i.e., Rutin, Nicotiflorin, Quercetin 3-beta-D-glucoside, and Hyperoside with the residues of ZIKV^{pro} as well as residues of ZIKV^{RdRp} domain along with the reference inhibitors, viz., O7N and sofosbuvir, respectively, were calculated at a total 30% interval of 100 ns simulation, which disclosed the significant binding of the respective ligands with the active site residues in the binding pocket (**Figure 8 and 9**).

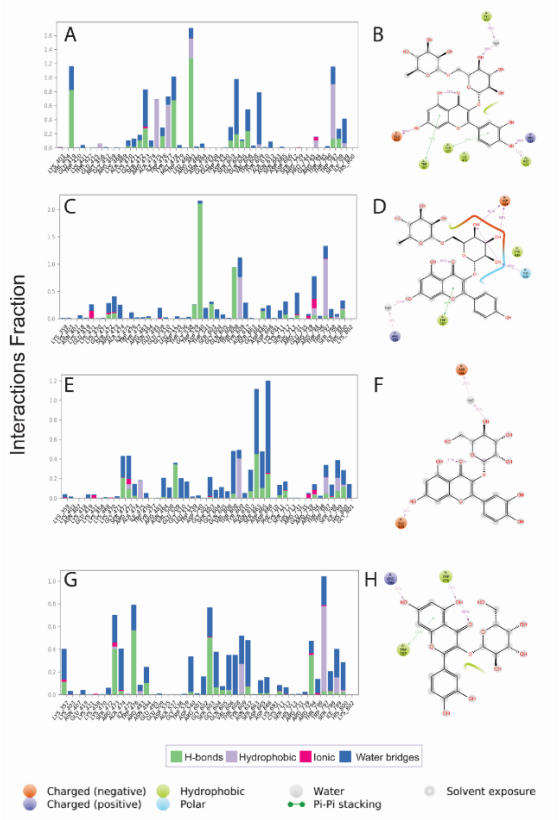

Figure 9. Protein-ligand interactions mapping for ZIKV^{RdRp} with selected natural compounds, i.e. **A-B.** Rutin, **C-D.** Nicotiflorin, **E-F.** Quercetin 3-beta-D-glucoside, and **G-H.** Hyperoside, extracted from 500 ns MD simulations. In 2D interaction diagram, the residues tyrosine, Valine, and Phenylalanine (green), arginine (violet), Aspartic acid (red), histidine and asparagine (blue), and glycine (grey) exhibit the hydrophobic, positive, negative, polar, and non-polar interactions, respectively along with hydrogen bonding (pink arrow) and pi-pi stacking (green line) with the receptor are extracted at 30% of the total MD simulation interaction interval.

Preprints (www.preprints.org) | NOT PEER-REVIEWED | Posted: 24 March 2022 doi:10.20944/preprints202203.0328.v1

3.5. Endpoint Free binding energy calculation

Molecular Mechanics Generalized Born Surface Area (MM/GBSA) was performed on the extracted poses from last 10 ns MD simulation trajectory of each docked complex to calculate the net binding free energy. Other energy components were also calculated, which are responsible for the stability of identified potential bioflavonoids docked in the binding pocket of viral proteins, i.e., $ZIKV^{pro}$ and $ZIKV^{RdRp}$. The net binding free energy of the screened bioflavonoids docked with the $ZIKV^{pro}$ was comparatively less negative concerning the reference $ZIKV^{pro}$-O7N docked complex but in a considerable range. In contrast, the net binding free energy for the screened bioflavonoids docked with the $ZIKV^{RdRp}$ was close to or more negative than the reference $ZIKV^{RdRp}$-Sofosbuvir docked complex. Interestingly, Rutin docked with the $ZIKV^{pro}$ and ZIKVRdRp showed high negative free binding energy compared to other identified bioflavonoids (**Table 2**).

Table 2. Endpoint binding free energy calculation of the selected bioflavonoids against $ZIKV^{pro}$ and $ZIKV^{RdRp}$ in comparison to the reference inhibitors.

S. No.	Compounds	Binding Free Energy (kcal/Mol)	
		$ZIKV^{pro}$	RdRp
1	Rutin	-57.094	-67.475
2	Nicotiflorin	-39.421	-60.847
3	Quercetin 3-beta-D-glucoside	-48.326	-54.15
4	Hyperoside	-44.538	-57.067
5	O7N (Control for $ZIKV^{pro}$)	-74.373	-
6	Sofosbuvir (control for $ZIKV^{RdRp}$)	-	-59.838

Additionally, the other energy components were also analyzed, and it was observed that in the case of $ZIKV^{pro}$-bioflavonoids docked complexes, Van der Waals interaction energy ($\Delta G_{Bind\ vdw}$) and, in $ZIKV^{RdRp}$-bioflavonoids docked complexes, $\Delta G_{Bind\ vdw}$ as well as Coulomb energy ($\Delta G_{Bind\ coloumb}$) were significantly contributing to the net binding affinity and stability of complexes (**Figure 10, Supplementary Figure S9, and Supplementary Tables S6 and S7**). Conclusively, these results suggest that the affinity and stability of $ZIKV^{pro}$ were higher for rutin, followed by Quercetin 3-beta-D-glucoside, Hyperoside, and Nicotiflorin in their respective order. In contrast, the stability and affinity of $ZIKV^{RdRp}$ were higher for Rutin followed by Nicotiflorin, Hyperoside, and Quercetin 3-beta-D-glucoside in their respective order. Hence, net binding free energy

Preprints (www.preprints.org) | NOT PEER-REVIEWED | Posted: 24 March 2022 doi:10.20944/preprints202203.0328.v1

calculated using MMGBSA analysis supports the screened four identified common bioflavonoids as putative inhibitors of viral proteins, viz. ZIKV^{pro} and ZIKV^{RdRp}.

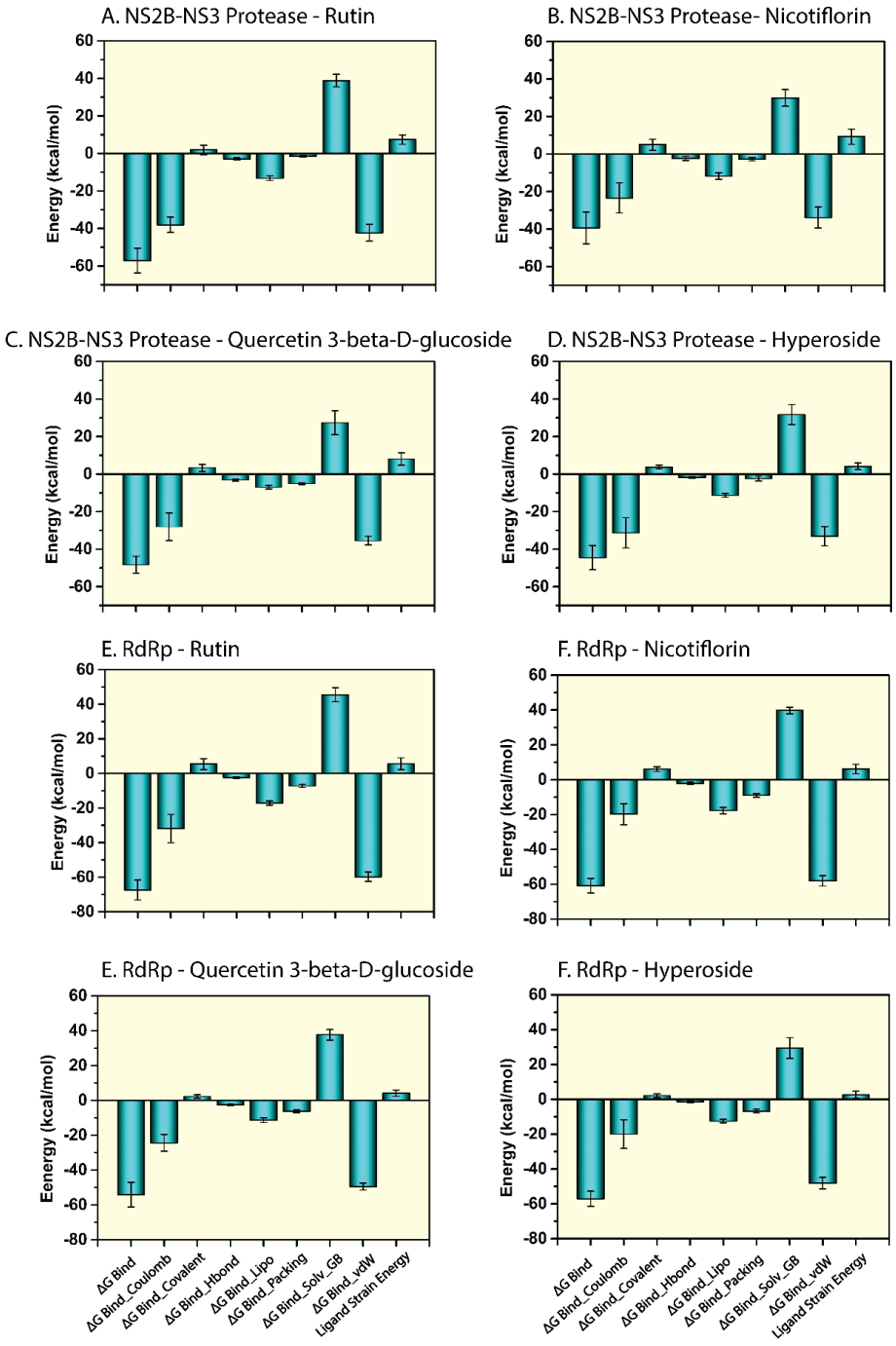

Figure 10. Calculated energy components and net MM/GBSA binding free energy (kcal/mol) with standard error values for extracted snapshots of docked complexes, i.e., **A.** ZIKV^{pro}-Rutin, **B.** ZIKV^{pro}-Nicotiflorin, **C.** ZIKV^{pro}- Quercetin 3-beta-D-glucoside, **D.** ZIKV^{pro}-Hyperoside, **E.** ZIKV^{RdRp}-Rutin, **F.** ZIKV^{RdRp}-Nicotiflorin, **G.** ZIKV^{RdRp}- Quercetin 3-beta-D-glucoside, **H.** ZIKV^{RdRp}-Hyperoside from respective 500 ns MD simulation trajectories.

Preprints (www.preprints.org) | NOT PEER-REVIEWED | Posted: 24 March 2022 doi:10.20944/preprints202203.0328.v1

4. Conclusion

The role of $ZIKV^{pro}$ and $ZIKV^{RdRp}$ in polyprotein processing and genome replication of ZIKV and lack of human homologs are the elementary regions to consider these proteins as molecular targets for the development of anti-ZIKV therapeutics. *Azadirachta indica* plant has placed itself in a category of natural resources with the best medicinal values. Therefore in this study, the reported bioflavonoids from *Azadirachta indica* were evaluated for their potential and therapeutic activity against the $ZIKV^{pro}$ and $ZIKV^{RdRp}$ domain using molecular simulations, drug-likeness, and endpoint binding free energy calculations. Notably, all the selected common bioflavonoids, i.e., Rutin, Nicotiflorin, Quercetin 3-beta-D-glucoside, and Hyperoside, among 44 bioactive compounds against the $ZIKV^{pro}$ and $ZIKV^{RdRp}$ exhibit substantially good binding affinity and dynamic stability. The screened compounds significantly occupied the binding pockets and depicted significant hydrogen and hydrophobic interactions along with pi-pi interactions with the essential residues of $ZIKV^{pro}$ and $ZIKV^{RdRp}$ against respective reference inhibitors. The analysis from MD simulation concluded that Rutin and Quercetin 3-beta-D-glucoside with minimum deviation was more stable, followed by Hyperoside and Nicotiflorin with $ZIKV^{pro,}$ and a similar pattern of stability were observed with the $ZIKV^{RdRp}$. At last, endpoint binding free energy calculation of the last ten poses from each docked complex also suggested Rutin and Quercetin 3-beta-D-glucoside potential compounds with higher MMGBSA scores. Overall, all four identified bioflavonoids showed significant stability and binding energy against $ZIKV^{pro}$ and $ZIKV^{RdRp}$, and further advised to validate these compounds through in vitro and in vivo experiments to develop potent therapeutics against Zika virus infection.

 doi:10.20944/preprints202203.0328.v1

Data availability

The datasets used and/or analyzed during the current study are available from the corresponding author on reasonable request.

Declaration of Competing Interest

The authors declare that they have no known competing financial interests or personal relationships that could have appeared to influence the work reported in this paper.

Acknowledgements:

The authors acknowledge the generous charitable donation from the late Sheikh Ibraheem Ahmed Azhar as a contribution to the scientific research community. Sanjay Kumar is the Council of Scientific and Industrial Research (CSIR) fellowship recipient. Also, the authors are thankful for the received technical support from the Institute of Biotechnology of the Czech Academy of Sciences (Institutional Research Concept, RVO: 86652036).

Author contributions

Conceptualization: VDD, SB, EIA, and SK; Methodology: SK, VDD, and SAEK; Data curation and Formal analysis: SK, SSM, SAEK, TAA, AAF, and AMK; Investigation: SK, VDD, SB, and EIA; Validation and Visualization: SSM, SAEK, TAA, AAF, and AMK; Roles/Writing - original draft: SK; Writing - review & editing: VDD, SB, SSM, and EIA; Supervision: VDD, SB, and EIA.

 doi:10.20944/preprints202203.0328.v1

References

[1] Dick GWA, Kitchen SF, Haddow AJ. Zika Virus (I). Isolations and serological specificity. Trans R Soc Trop Med Hyg 1952;46:509–20. https://doi.org/10.1016/0035-9203(52)90042-4.

[2] Duffy MR, Chen T-H, Hancock WT, Powers AM, Kool JL, Lanciotti RS, et al. Zika Virus Outbreak on Yap Island, Federated States of Micronesia. N Engl J Med 2009;360:2536–43. https://doi.org/10.1056/nejmoa0805715.

[3] Musso D, Nilles EJ, Cao-Lormeau VM. Rapid spread of emerging Zika virus in the Pacific area. Clin Microbiol Infect 2014;20:O595–6. https://doi.org/10.1111/1469-0691.12707.

[4] Van-Mai Cao-Lormeau, Claudine Roche, Anita Teissier, Emilie Robin, Anne-Laure Berry, Henri-Pierre Mallet, Amadou Alpha Sall DM. Zika Virus, French Polynesia, South Pacific. Emerg Infect Dis 2014. https://doi.org/10.3201/eid2006.140138.

[5] Hennessey M, Fischer M, Staples JE. Zika Virus Spreads to New Areas - Region of the Americas, May 2015-January 2016. Am J Transplant 2016;16:1031–4. https://doi.org/10.1111/ajt.13743.

[6] World Health Organization, "Zika virus, microcephaly and Guillain–Barre´ syndrome," WHO, Geneva, Switzerland, September, 2016, http://www.who.int/emergencies/zikavirus/situation-report/1-september-2016/en/ 2016:1–15.

[7] Torres JR, Murillo J, Bofill L. The ever changing landscape of Zika virus infection. Learning on the fly. Int J Infect Dis 2016;51:123–6. https://doi.org/10.1016/j.ijid.2016.09.001.

[8] Sabrina Tavernise. CDC Investigating 14 New Reports of Zika Transmission Through Sex. New York Times 2016.

[9] Musso D, Roche C, Robin E, Nhan T, Teissier A, Cao-Lormeau V-M. Potential sexual transmission of Zika virus. Emerg Infect Dis 2015;21:359–61. https://doi.org/10.3201/eid2102.141363.

[10] Vasilakis N, Weaver SC. Flavivirus transmission focusing on Zika. Curr Opin Virol 2017;22:30–5. https://doi.org/10.1016/j.coviro.2016.11.007.

[11] Driggers RW, Ho C-Y, Korhonen EM, Kuivanen S, Jääskeläinen AJ, Smura T, et al. Zika Virus Infection With Prolonged Maternal Viremia and Fetal Brain Abnormalities. Obstet Anesth Dig 2017;37:51–51. https://doi.org/10.1097/01.aoa.0000512046.09676.84.

[12] Petersen E, Wilson ME, Touch S, McCloskey B, Mwaba P, Bates M, et al. Rapid Spread of Zika Virus in The Americas - Implications for Public Health Preparedness for Mass Gatherings at the 2016 Brazil Olympic Games. Int J Infect Dis 2016;44:11–5. https://doi.org/10.1016/j.ijid.2016.02.001.

[13] Brasil P, Pereira JPJ, Moreira ME, Ribeiro Nogueira RM, Damasceno L, Wakimoto M, et al. Zika Virus Infection in Pregnant Women in Rio de Janeiro. N Engl J Med 2016;375:2321–34. https://doi.org/10.1056/NEJMoa1602412.

[14] Kuno G, Chang G-JJ. Full-length sequencing and genomic characterization of Bagaza, Kedougou, and Zika viruses. Arch Virol 2007;152:687–96. https://doi.org/10.1007/s00705-006-0903-z.

[15] Lindenbach BD, Rice CM. Molecular biology of flaviviruses. Adv Virus Res 2003;59:23–61. https://doi.org/10.1016/s0065-3527(03)59002-9.

[16] Yu I-M, Zhang W, Holdaway HA, Li L, Kostyuchenko VA, Chipman PR, et al. Structure of the Immature Dengue Virus at Low pH Primes Proteolytic Maturation. Science (80-) 2008;319:1834 LP – 1837. https://doi.org/10.1126/science.1153264.

[17] Wang A, Thurmond S, Islas L, Hui K, Hai R. Zika virus genome biology and molecular pathogenesis. Emerg Microbes Infect 2017;6:e13. https://doi.org/10.1038/emi.2016.141.

[18] Chappell K, Stoermer M, Fairlie D, Young P. West Nile Virus NS2B/NS3 Protease As An Antiviral Target. Curr Med Chem 2008;15:2771–84. https://doi.org/10.2174/092986708786242804.

[19] Yildiz M, Ghosh S, A. Bell J, Sherman W, A. Hardy J. Allosteric Inhibition of the NS2B-NS3 Protease from Dengue Virus. ACS Chem Biol 2013;8:2744–52. https://doi.org/10.1021/cb400612h.

[20] Shiryaev SA, Kozlov IA, Ratnikov BI, Smith JW, Lebl M, Strongin AY. Cleavage preference distinguishes the two-component NS2B-NS3 serine proteinases of Dengue and West Nile viruses.

Biochem J 2007;401:743–52. https://doi.org/10.1042/BJ20061136.

[21] Leung D, Schroder K, White H, Fang NX, Stoermer MJ, Abbenante G, et al. Activity of recombinant dengue 2 virus NS3 protease in the presence of a truncated NS2B cofactor, small peptide substrates, and inhibitors. J Biol Chem 2001;276:45762–71. https://doi.org/10.1074/jbc.M107360200.

[22] Erbel P, Schiering N, D'Arcy A, Renatus M, Kroemer M, Lim SP, et al. Structural basis for the activation of flaviviral NS3 proteases from dengue and West Nile virus. Nat Struct Mol Biol 2006;13:372–3. https://doi.org/10.1038/nsmb1073.

[23] Yusof R, Clum S, Wetzel M, Murthy HM, Padmanabhan R. Purified NS2B/NS3 serine protease of dengue virus type 2 exhibits cofactor NS2B dependence for cleavage of substrates with dibasic amino acids in vitro. J Biol Chem 2000;275:9963–9. https://doi.org/10.1074/jbc.275.14.9963.

[24] Li Y, Loh YR, Hung AW, Kang C. Characterization of molecular interactions between Zika virus protease and peptides derived from the C-terminus of NS2B. Biochem Biophys Res Commun 2018;503:691–6. https://doi.org/10.1016/j.bbrc.2018.06.062.

[25] Clum S, Ebner KE, Padmanabhan R. Cotranslational membrane insertion of the serine proteinase precursor NS2B-NS3(Pro) of dengue virus type 2 is required for efficient in vitro processing and is mediated through the hydrophobic regions of NS2B. J Biol Chem 1997;272:30715–23. https://doi.org/10.1074/jbc.272.49.30715.

[26] Aktepe TE, Mackenzie JM. Shaping the flavivirus replication complex: It is curvaceous! Cell Microbiol 2018;20:e12884. https://doi.org/10.1111/cmi.12884.

[27] Lescar J, Soh S, Lee LT, Vasudevan SG, Kang C, Lim SP. The Dengue Virus Replication Complex: From RNA Replication to Protein-Protein Interactions to Evasion of Innate Immunity BT - Dengue and Zika: Control and Antiviral Treatment Strategies. In: Hilgenfeld R, Vasudevan SG, editors., Singapore: Springer Singapore; 2018, p. 115–29. https://doi.org/10.1007/978-981-10-8727-1_9.

[28] Ngo AM, Shurtleff MJ, Popova KD, Kulsuptrakul J, Weissman JS, Puschnik AS. The ER membrane protein complex is required to ensure correct topology and stable expression of flavivirus polyproteins. Elife 2019;8. https://doi.org/10.7554/eLife.48469.

[29] Welsch S, Miller S, Romero-brey I, Merz A, Bleck CKE, Walther P, et al. Article Composition and Three-Dimensional Architecture of the Dengue Virus Replication and Assembly Sites. Cell Host Microbe 2009;5:365–75. https://doi.org/10.1016/j.chom.2009.03.007.

[30] Zhenzhen Z, Yan L, Ru LY, Wint PW, W. HA, CongBao K, et al. Crystal structure of unlinked NS2B-NS3 protease from Zika virus. Science (80-) 2016;354:1597–600. https://doi.org/10.1126/science.aai9309.

[31] Phoo WW, Li Y, Zhang Z, Lee MY, Loh YR, Tan YB, et al. Structure of the NS2B-NS3 protease from Zika virus after self-cleavage. Nat Commun 2016;7:1–8. https://doi.org/10.1038/ncomms13410.

[32] Li Y, Zhang Z, Phoo WW, Loh YR, Li R, Yang HY, et al. Structural Insights into the Inhibition of Zika Virus NS2B-NS3 Protease by a Small-Molecule Inhibitor. Structure 2018;26:555-564.e3. https://doi.org/https://doi.org/10.1016/j.str.2018.02.005.

[33] Li Y, Zhang Z, Phoo WW, Loh YR, Wang W, Liu S, et al. Structural Dynamics of Zika Virus NS2B-NS3 Protease Binding to Dipeptide Inhibitors. Structure 2017;25:1242-1250.e3. https://doi.org/10.1016/j.str.2017.06.006.

[34] Quek JP, Liu S, Zhang Z, Li Y, Ng EY, Loh YR, et al. Identification and structural characterization of small molecule fragments targeting Zika virus NS2B-NS3 protease. Antiviral Res 2020;175:104707. https://doi.org/10.1016/j.antiviral.2020.104707.

[35] Li Y, Phoo WW, Loh YR, Zhang Z, Ng EY, Wang W, et al. Structural characterization of the linked NS2B-NS3 protease of Zika virus. FEBS Lett 2017;591:2338–47. https://doi.org/10.1002/1873-3468.12741.

[36] Li Q, Kang C. Structure and Dynamics of Zika Virus Protease and Its Insights into Inhibitor Design.

Biomedicines 2021;9. https://doi.org/10.3390/biomedicines9081044.
[37] Hilgenfeld R, Lei J, Zhang L. The Structure of the Zika Virus Protease, NS2B/NS3(pro). Adv Exp Med Biol 2018;1062:131–45. https://doi.org/10.1007/978-981-10-8727-1_10.
[38] Zhao B, Yi G, Du F, Chuang Y-C, Vaughan RC, Sankaran B, et al. Structure and function of the Zika virus full-length NS5 protein. Nat Commun 2017;8:14762. https://doi.org/10.1038/ncomms14762.
[39] Zhao Y, Soh TS, Lim SP, Chung KY, Swaminathan K, Vasudevan SG, et al. Molecular basis for specific viral RNA recognition and 2′-O-ribose methylation by the dengue virus nonstructural protein 5 (NS5). Proc Natl Acad Sci U S A 2015;112:14834–9. https://doi.org/10.1073/pnas.1514978112.
[40] Upadhyay AK, Cyr M, Longenecker K, Tripathi R, Sun C, Kempf DJ. Crystal structure of full-length Zika virus NS5 protein reveals a conformation similar to Japanese encephalitis virus NS5. Acta Crystallogr Sect F, Struct Biol Commun 2017;73:116–22. https://doi.org/10.1107/S2053230X17001601.
[41] Valente AP, Moraes AH. Zika virus proteins at an atomic scale: how does structural biology help us to understand and develop vaccines and drugs against Zika virus infection? J Venom Anim Toxins Incl Trop Dis 2019;25:e20190013–e20190013. https://doi.org/10.1590/1678-9199-JVATITD-2019-0013.
[42] Wang B, Tan X-F, Thurmond S, Zhang Z-M, Lin A, Hai R, et al. The structure of Zika virus NS5 reveals a conserved domain conformation. Nat Commun 2017;8:14763. https://doi.org/10.1038/ncomms14763.
[43] Wang B, Thurmond S, Hai R, Song J. Structure and function of Zika virus NS5 protein: perspectives for drug design. Cell Mol Life Sci 2018;75:1723–36. https://doi.org/10.1007/s00018-018-2751-x.
[44] Li Z, Sakamuru S, Huang R, Brecher M, Koetzner CA, Zhang J, et al. Erythrosin B is a potent and broad-spectrum orthosteric inhibitor of the flavivirus NS2B-NS3 protease. Antiviral Res 2018;150:217–25. https://doi.org/https://doi.org/10.1016/j.antiviral.2017.12.018.
[45] Li Z, Brecher M, Deng YQ, Zhang J, Sakamuru S, Liu B, et al. Existing drugs as broad-spectrum and potent inhibitors for Zika virus by targeting NS2B-NS3 interaction. Cell Res 2017;27:1046–64. https://doi.org/10.1038/cr.2017.88.
[46] M. B, Z. L, B. L, J. Z, CA K, A. A, et al. A conformational switch high-throughput screening assay and allosteric inhibition of the flavivirus NS2B-NS3 protease. PLoS Pathog 2017;13:1–29.
[47] Nitsche C, Passioura T, Varava P, Mahawaththa MC, Leuthold MM, Klein CD, et al. De Novo Discovery of Nonstandard Macrocyclic Peptides as Noncompetitive Inhibitors of the Zika Virus NS2B-NS3 Protease. ACS Med Chem Lett 2019;10:168–74. https://doi.org/10.1021/acsmedchemlett.8b00535.
[48] Millies B, Von Hammerstein F, Gellert A, Hammerschmidt S, Barthels F, Göppel U, et al. Proline-Based Allosteric Inhibitors of Zika and Dengue Virus NS2B/NS3 Proteases. J Med Chem 2019;62:11359–82. https://doi.org/10.1021/acs.jmedchem.9b01697.
[49] Lei J, Hansen G, Nitsche C, Klein CD, Zhang L, Hilgenfeld R. Crystal structure of zika virus ns2b-ns3 protease in complex with a boronate inhibitor. Science (80-) 2016;353:503–5. https://doi.org/10.1126/science.aag2419.
[50] Li Y, Zhang Z, Phoo WW, Loh YR, Wang W, Liu S, et al. Structural Dynamics of Zika Virus NS2B-NS3 Protease Binding to Dipeptide Inhibitors. Structure 2017;25:1242-1250.e3. https://doi.org/10.1016/j.str.2017.06.006.
[51] Nitsche C, Zhang L, Weigel LF, Schilz J, Graf D, Bartenschlager R, et al. Peptide-Boronic Acid Inhibitors of Flaviviral Proteases: Medicinal Chemistry and Structural Biology. J Med Chem 2017;60:511–6. https://doi.org/10.1021/acs.jmedchem.6b01021.
[52] Ramharack P, Soliman MES. Zika virus NS5 protein potential inhibitors: an enhanced in silico approach in drug discovery. J Biomol Struct Dyn 2018;36:1118–33. https://doi.org/10.1080/07391102.2017.1313175.

[53] Aicha G-A, Sridhar S, Hwa WY, K. CKW, Thing TS, W. BR, et al. Non-nucleoside Inhibitors of Zika Virus RNA-Dependent RNA Polymerase. J Virol 2021;94:e00794-20. https://doi.org/10.1128/JVI.00794-20.

[54] Noreen, Ali R, Badshah SL, Faheem M, Abbasi SW, Ullah R, et al. Identification of potential inhibitors of Zika virus NS5 RNA-dependent RNA polymerase through virtual screening and molecular dynamic simulations. Saudi Pharm J 2020;28:1580–91. https://doi.org/https://doi.org/10.1016/j.jsps.2020.10.005.

[55] Song W, Zhang H, Zhang Y, Chen Y, Lin Y, Han Y, et al. Identification and Characterization of Zika Virus NS5 Methyltransferase Inhibitors. Front Cell Infect Microbiol 2021;11:1–10. https://doi.org/10.3389/fcimb.2021.665379.

[56] Xu M, Lee EM, Wen Z, Cheng Y, Huang WK, Qian X, et al. Identification of small-molecule inhibitors of Zika virus infection and induced neural cell death via a drug repurposing screen. Nat Med 2016;22:1101–7. https://doi.org/10.1038/nm.4184.

[57] Kuivanen S, Bespalov MM, Nandania J, Ianevski A, Velagapudi V, De Brabander JK, et al. Obatoclax, saliphenylhalamide and gemcitabine inhibit Zika virus infection in vitro and differentially affect cellular signaling, transcription and metabolism. Antiviral Res 2017;139:117–28. https://doi.org/10.1016/j.antiviral.2016.12.022.

[58] Tan CW, Sam IC, Chong WL, Lee VS, Chan YF. Polysulfonate suramin inhibits Zika virus infection. Antiviral Res 2017;143:186–94. https://doi.org/10.1016/j.antiviral.2017.04.017.

[59] Yuan S, Chan JFW, den-Haan H, Chik KKH, Zhang AJ, Chan CCS, et al. Structure-based discovery of clinically approved drugs as Zika virus NS2B-NS3 protease inhibitors that potently inhibit Zika virus infection in vitro and in vivo. Antiviral Res 2017;145:33–43. https://doi.org/10.1016/j.antiviral.2017.07.007.

[60] Talevi A. Multi-target pharmacology: possibilities and limitations of the "skeleton key approach" from a medicinal chemist perspective . Front Pharmacol 2015;6:205.

[61] Makhoba XH, Viegas Jr C, Mosa RA, Viegas FPD, Pooe OJ. Potential Impact of the Multi-Target Drug Approach in the Treatment of Some Complex Diseases. Drug Des Devel Ther 2020;14:3235–49. https://doi.org/10.2147/DDDT.S257494.

[62] Li YH, Wang PP, Li XX, Yu CY, Yang H, Zhou J, et al. The Human Kinome Targeted by FDA Approved Multi-Target Drugs and Combination Products: A Comparative Study from the Drug-Target Interaction Network Perspective. PLoS One 2016;11:e0165737. https://doi.org/10.1371/journal.pone.0165737.

[63] Subapriya R, Nagini S. Medicinal properties of neem leaves: a review. Curr Med Chem Anticancer Agents 2005;5:146–9. https://doi.org/10.2174/1568011053174828.

[64] Gupta SC, Prasad S, Tyagi AK, Kunnumakkara AB, Aggarwal BB. Neem (Azadirachta indica): An indian traditional panacea with modern molecular basis. Phytomedicine 2017;34:14–20. https://doi.org/https://doi.org/10.1016/j.phymed.2017.07.001.

[65] Yadav DK, Bharitkar YP, Chatterjee K, Ghosh M, Mondal NB, Swarnaka S. Importance of Neem Leaf: An insight into its role in combating diseases. Indian J Exp Biol 2016;54:708–18.

[66] Braun NJ, Quek JP, Huber S, Kouretova J, Rogge D, Lang-Henkel H, et al. Structure-Based Macrocyclization of Substrate Analogue NS2B-NS3 Protease Inhibitors of Zika, West Nile and Dengue viruses. ChemMedChem 2020;15:1439–52. https://doi.org/10.1002/cmdc.202000237.

[67] Gharbi-Ayachi A, Santhanakrishnan S, Wong YH, Chan KWK, Tan ST, Bates RW, et al. Non-nucleoside Inhibitors of Zika Virus RNA-Dependent RNA Polymerase. J Virol 2020;94. https://doi.org/10.1128/JVI.00794-20.

[68] Berman HM, Westbrook J, Feng Z, Gilliland G, Bhat TN, Weissig H, et al. The Protein Data Bank. Nucleic Acids Res 2000;28:235–42. https://doi.org/10.1093/nar/28.1.235.

[69] Schrödinger Release 2018-4: Protein Preparation Wizard; Epik, Schrödinger, LLC, New York, NY,

2018 n.d.
[70] Kim S, Thiessen PA, Bolton EE, Chen J, Fu G, Gindulyte A, et al. PubChem Substance and Compound databases. Nucleic Acids Res 2016;44:D1202–13. https://doi.org/10.1093/nar/gkv951.
[71] Aicha G-A, Sridhar S, Hwa WY, K. CKW, Thing TS, W. BR, et al. Non-nucleoside Inhibitors of Zika Virus RNA-Dependent RNA Polymerase. J Virol 2021;94:e00794-20. https://doi.org/10.1128/JVI.00794-20.
[72] Sacramento CQ, de Melo GR, de Freitas CS, Rocha N, Hoelz LVB, Miranda M, et al. The clinically approved antiviral drug sofosbuvir inhibits Zika virus replication. Sci Rep 2017;7:40920. https://doi.org/10.1038/srep40920.
[73] Daina A, Michielin O, Zoete V. SwissADME: a free web tool to evaluate pharmacokinetics, drug-likeness and medicinal chemistry friendliness of small molecules. Sci Rep 2017;7. https://doi.org/10.1038/SREP42717.
[74] Cheng F, Li W, Zhou Y, Shen J, Wu Z, Liu G, et al. admetSAR: a comprehensive source and free tool for assessment of chemical ADMET properties. J Chem Inf Model 2012;52:3099–105. https://doi.org/10.1021/ci300367a.
[75] Lin Y, Zhang H, Song W, Si S, Han Y, Jiang J. Identification and characterization of Zika virus NS5 RNA-dependent RNA polymerase inhibitors. Int J Antimicrob Agents 2019;54:502–6. https://doi.org/10.1016/j.ijantimicag.2019.07.010.
[76] Bowers KJ, Chow E, Xu H, Dror RO, Eastwood MP, Gregersen BA, et al. Scalable Algorithms for Molecular Dynamics Simulations on Commodity Clusters. Proc. 2006 ACM/IEEE Conf. Supercomput., New York, NY, USA: Association for Computing Machinery; 2006, p. 84–es. https://doi.org/10.1145/1188455.1188544.
[77] Schrödinger Release 2020-4: Desmond Molecular Dynamics System, D. E. Shaw Research, New York, NY, 2020. Maestro-Desmond Interoperability Tools, Schrödinger, New York, NY, 2020. n.d.
[78] Negahdari R, Bohlouli S, Sharifi S, Maleki Dizaj S, Rahbar Saadat Y, Khezri K, et al. Therapeutic benefits of rutin and its nanoformulations. Phytother Res 2021;35:1719–38. https://doi.org/10.1002/ptr.6904.
[79] Caparica R, Júlio A, Araújo MEM, Baby AR, Fonte P, Costa JG, et al. Anticancer Activity of Rutin and Its Combination with Ionic Liquids on Renal Cells. Biomolecules 2020;10. https://doi.org/10.3390/biom10020233.
[80] Budzynska B, Faggio C, Kruk-Slomka M, Samec D, Nabavi SF, Sureda A, et al. Rutin as Neuroprotective Agent: From Bench to Bedside. Curr Med Chem 2019;26:5152–64. https://doi.org/10.2174/0929867324666171003114154.
[81] Habtemariam S. Rutin as a Natural Therapy for Alzheimer's Disease: Insights into its Mechanisms of Action. Curr Med Chem 2016;23:860–73. https://doi.org/10.2174/0929867323666160217124333.
[82] Shaik YB, Castellani ML, Perrella A, Conti F, Salini V, Tete S, et al. Role of quercetin (a natural herbal compound) in allergy and inflammation. J Biol Regul Homeost Agents 2006;20:47–52.
[83] Thapa M, Kim Y, Desper J, Chang K-O, Hua DH. Synthesis and antiviral activity of substituted quercetins. Bioorg Med Chem Lett 2012;22:353–6. https://doi.org/10.1016/j.bmcl.2011.10.119.
[84] Savov VM, Galabov AS, Tantcheva LP, Mileva MM, Pavlova EL, Stoeva ES, et al. Effects of rutin and quercetin on monooxygenase activities in experimental influenza virus infection. Exp Toxicol Pathol Off J Gesellschaft Fur Toxikologische Pathol 2006;58:59–64. https://doi.org/10.1016/j.etp.2006.05.002.
[85] Habtemariam S, Lentini G. The therapeutic potential of rutin for diabetes: an update. Mini Rev Med Chem 2015;15:524–8. https://doi.org/10.2174/1389557515070150424103721.
[86] Bharadwaj S, Dubey A, Yadava U, Mishra SK, Kang SG, Dwivedi VD. Exploration of natural compounds with anti-SARS-CoV-2 activity via inhibition of SARS-CoV-2 Mpro. Brief Bioinform 2021;22:1361–77. https://doi.org/10.1093/bib/bbaa382.

[87] Dubey R, Dubey K. Molecular Docking Studies of Bioactive Nicotiflorin against 6W63 Novel Coronavirus 2019 (COVID-19). Comb Chem High Throughput Screen 2021;24:874–8. https://doi.org/10.2174/1386207323999200820162551.

[88] Hu Z, Zhao P, Xu H. Hyperoside exhibits anticancer activity in non-small cell lung cancer cells with T790M mutations by upregulating FoxO1 via CCAT1. Oncol Rep 2020;43:617–24. https://doi.org/10.3892/or.2019.7440.

[89] Kong Y, Sun W, Wu P. Hyperoside exerts potent anticancer activity in skin cancer. Front Biosci (Landmark Ed 2020;25:463–79. https://doi.org/10.2741/4814.

[90] Dwivedi VD, Singh A, El-Kafraway SA, Alandijany TA, Faizo AA, Bajrai LH, et al. Mechanistic insights into the Japanese encephalitis virus RNA dependent RNA polymerase protein inhibition by bioflavonoids from Azadirachta indica. Sci Rep 2021;11:18125. https://doi.org/10.1038/s41598-021-96917-0.

[91] Hay M, Thomas DW, Craighead JL, Economides C, Rosenthal J. Clinical development success rates for investigational drugs. Nat Biotechnol 2014;32:40–51. https://doi.org/10.1038/nbt.2786.

[92] Macarron R. Critical review of the role of HTS in drug discovery. Drug Discov Today 2006;11:277–9. https://doi.org/10.1016/j.drudis.2006.02.001.

[93] Lipinski CA. Lead- and drug-like compounds: the rule-of-five revolution. Drug Discov Today Technol 2004;1:337–41. https://doi.org/10.1016/j.ddtec.2004.11.007.